Materials & Design 254 (2025) 114051

Contents lists available at ScienceDirect

Materials & Design

journal homepage: www.elsevier.com/locate/matdes

Engineering low clinker Strain-Hardening cementitious composites (SHCC) using polyethylene and cost-effective polypropylene fibers: An experimental scale-linking analysis

Ameer Hamza Ahmed [a], Julia Hübner [b], Dominik Junger [a], Cesare Signorini [a,*], Marko Butler [a], Marco Liebscher [b,*], Christina Scheffler [b], Viktor Mechtcherine [a]

[a] Institute of Construction Materials, TU Dresden 01062 Dresden, Germany
[b] Leibniz-Institut für Polymerforschung Dresden e. V., Hohe Straße 6, 01069 Dresden, Germany

ARTICLE INFO

Keywords:
LC^3
SHCC
Clinker factor
DIC
Polypropylene
Polyethylene
Strain-hardening
Scale-linking

ABSTRACT

This paper reports on an experimental scale-linking study aimed at the design and mechanical characterization of low-clinker and cost-efficient strain-hardening cementitious composites (SHCC). Three distinct matrices were examined, each comprising a limestone calcined clay cement (LC^3) binder with reduced Portland cement (PC) contents of 50 %, 35 %, and 25 %. These fine-grained matrices were reinforced with cost-effective and low-tenacity polypropylene (PP) fibers, while high-performance and expensive polyethylene (PE) fibers were used as a benchmark. Various micro-, meso-, and macro-scale mechanical and analytical tests were performed after 28 days of curing age, including single fiber pull-out, uniaxial tensile testing on notched and unnotched specimens, flexure, compression testing, digital image correlation analysis, and environmental scanning electron microscopy. The results clearly showed that the low tensile strength and high compliance of PP, when combined with a low-strength matrix containing only 25 wt% PC, contributed to better strain-hardening behavior, attributed to the fine-tuning of the micromechanical design of the interacting phases. Naturally, such a design significantly enhances the sustainability credentials of SHCC while at the same time increasing its cost-saving potential, evening out the response of high-performance and costly PE fibers incorporated into a high-strength matrix (*e.g.*, with 50 wt% PC).

1. Introduction

Strain-hardening cementitious composites (SHCC), or engineered cementitious composites (ECC), are a special class of short fiber reinforced composites (FRC). Emerging in the early 1990s [1], SHCC are recognized for improving structural performance and overcoming the critical shortcomings of traditional concrete: brittleness, limited tensile strength, poor crack width control, the need for thick structural elements, and the abrupt failure mode under dynamic loading events. The formulation of SHCC consists of 2–3 % by volume of short polymer fibers, randomly dispersed in a fine-grained mineral-bonded (*i.e.*, generally cementitious) matrix. When subjected to tensile loading, SHCC exhibit significant inelastic deformations while experiencing an increase in load-bearing capacity after initial crack formation. This so-called strain-hardening phenomenon is due to the formation of multiple microcracks orthogonal to the loading direction, with each crack effectively bridged by the embedded fibers. Crack bridging ensures that the applied load is distributed to the undamaged matrix regions by the fibers in the crack flanks. As a result, SHCC exhibit exceptional tensile quasi-ductility, exceeding that of conventional concrete by several hundred times [2,3].

The design philosophy of SHCC is deeply rooted in micromechanical principles that depend on the interactions between its constituents, *i.e.*, fibers, matrix, and their interfaces [4]. The framework underlying the mechanical response of SHCC is based on a multiscale conceptual approach, which establishes a hierarchical connections between different scales describing different facets of material behavior. At the micro-scale (*nm-μm*), the single fiber/matrix interface governs fundamental load transfer mechanisms. At the meso-scale (*μm-mm*), these interactions influence matrix cracking properties and fiber bridging behavior within individual cracks. At the macro-scale (*mm-cm*), the sequential formation of multiple steady-state cracks determines the

* Corresponding authors.
E-mail addresses: cesare.signorini@tu-dresden.de (C. Signorini), marco.liebscher@tu-dresden.de (M. Liebscher).

https://doi.org/10.1016/j.matdes.2025.114051
Received 30 September 2024; Received in revised form 7 March 2025; Accepted 4 May 2025
Available online 5 May 2025

overall tensile strain-hardening behavior and fracture processes of the composite [5]. Linking scales in the analysis of SHCC is pivotal to intertwining its/their holistic mechanical behavior to micromechanical features and mechanisms.

By tailoring these phases, a wide variety of SHCC can be developed that are suitable for many applications [6–8]. Numerous research works have demonstrated the superior efficiency of SHCC formulations based on different matrix and fiber combinations for general repair and retrofit of existing structures [9–12] and for strengthening against seismic loads [13,14], impact, or blast loads [15–19].

Despite the numerous advantages of SHCC, its environmental and economic viability is frequently called into question. Li [20] linked the high carbon footprint and cost of SHCC to the higher cement content compared to ordinary concrete and the use of high-performance polymer fibers. The high cement content stems from the absence of coarse aggregates and inflates the cost of SHCC and, above all, its environmental footprint. To mitigate this criticality, high-volume substitutions of supplementary cementitious materials (SCMs) are often endorsed in the mix design of SHCC, replacing a portion of Portland cement (PC). SCMs are generally more affordable and entail a significantly lower CO_2 footprint than PC. However, conventional SCMs, such as fly ash, ground-granulated blast furnace slag, silica fume, *etc.*, are gradually becoming scarce due to the transition in the energy and industrial sectors towards more sustainable processes. In recent years, an innovative replacement for PC, limestone calcined clay cement (LC^3), has emerged as a sustainable and long-lasting solution in the field of construction [21–23]. LC^3 capitalizes on the pozzolanic characteristics of readily accessible kaolinitic clays, activated through calcination (calcined clays, or CC) in conjunction with limestone (LS) and a modest quantity of gypsum.

To date, a limited number of research studies have attempted to partially replace PC with the combination of LS and CC to obtain ternary LC^3-based SHCC [24–31]. In some studies, other SCMs, such as fly ash [24,28] and silica fume [25,30], were retained in the mixture, resulting in a quaternary binder-based SHCC. Results show that LC^3-based SHCC can generally achieve similar and, oftentimes, even better tensile strength and strain capacity than comparable SHCC counterparts devoid of LC^3 while remarkably reducing CO_2 emissions compared to traditional concrete and FA-SHCC [24,28,31]. Notwithstanding these environmental benefits, the design of blended binders offers only marginal cost advantages over conventional SHCC, as the cost of high-performance fibers plays the most prominent role. Recent research by Liao *et al.* [32] has demonstrated that over 36 % of the cost of SHCC is attributable to the utilization of PE fibers. Although PVA fibers, which are eight times less cost-intensive than PE fibers, are also commonly utilized, their strong hydrophilic nature hinders the strain capacities of SHCC. Additional surface treatments, such as oil coating, are often required to make them suitable for pseudo-ductile SHCC [33]. This reduces their appeal and cost-effectiveness in practical applications.

In the search for more economical alternatives, polyethylene terephthalate (PET) and polypropylene (PP) fibers have received much attention. These are some of the most synthesized fibers globally [34,35], widely available, cost-effective, and highly recyclable [36]. In the European market, PET and PP fibers offer up to 95 % cost savings over the ultra-high molecular weight polyethylene (UHMWPE, here used as PE) fibers considered in this study. Most of the cost savings for PP and PET are due to their melt-spinning production method, which is less energy-intensive and does not require additional chemicals such as solvents during production. This leads to easier and more environmentally friendly manufacturing processes for PP and PET compared to PE fibers [37].

A previous investigation by the authors demonstrated the efficacy of PET-reinforced LC^3-based SHCC [38], indicating that the composite based on an LC^3 matrix including 25 % PC content by weight exhibited a tensile strength (3.3 MPa) and strain capacities exceeding 4 %. The present study shifts its focus towards low-tenacity (standard) PP fibers. A handful of studies have demonstrated the strain-hardening capability using high-tenacity PP (HTPP), with strain capacities exceeding 2 % [39–42]. However, it should be noted that the enhanced mechanical performance of HTPP compared to standard PP fibers is achieved through a more sophisticated manufacturing process, involving high-temperature spinning and drawing, delayed quenching, and moderate draw ratios [43,44]. This also affects the availability and cost of HTPP.

Notably, the compliant nature of fibers such as PP and PET provides significant advantages in dynamic loading conditions, including seismic events, impact forces, and blast loading. These fibers exhibit high plastic deformation within crack flanks, promoting substantial energy dissipation through fiber yielding. This dissipation can be further enhanced by promoting fiber yielding not only within a single crack but across multiple cracks in the composite. As a result, the development of SHCC incorporating compliant fibers represents a promising strategy for improving structural resilience under dynamic loads. Furthermore, the hydrophobic nature of these fibers leads to additional energy dissipation during the fiber pull-out process from cracked flanks. Due to these reasons, composites made of such fibers when applied as thin strengthening layers on existing critical infrastructure can significantly enhance impact resistance and overall structural safety [45].

When standard PP fibers are employed in fiber-reinforced concrete, strain-softening tensile and flexural post-peak behavior is often observed due to their low tensile strengths. Furthermore, PP or HTPP is hydrophobic and characterized by smooth fiber surfaces, resulting in a weak fiber/matrix interaction [46,47]. Accordingly, one of the principal criteria for achieving strain hardening when utilizing standard PP fibers is that the matrix strength must be less than the minimum crack-bridging strength of the PP fibers [1,4,39,48]. It is thus challenging to design SHCC with standard PP fibers and requires veering to less dense matrices for reduced matrix cracking strength, a decision that, in turn, further constrains the fiber/matrix interfacial properties and, consequently, their crack-bridging capacity. As mentioned above, fly ash has historically driven the mix design of SHCC matrices. Its spherical particle morphology introduces the "*ball-bearing effect*" [49,50], which, while improving fiber dispersion, limits the mechanical interlocking of the fibers with the matrix. In this regard, LC^3 can be a convenient and beneficial addition, as CC and LS, due to their irregular particle shapes [51], can enhance the mechanical interactions between smooth PP fibers and the matrix. This is particularly advantageous when high volumes of these SCMs are utilized to replace PC, ensuring their presence at the fiber/matrix interface while maintaining low matrix strength due to high PC replacement levels.

In view of these delicate phase interactions in SHCC systems, the present study focuses on three diluted (high PC replacement levels) LC^3 matrix formulations that have been identified as suitable for achieving tensile strain hardening with low-strength and compliant PP fibers. The objective is to enhance the sustainability and financial credentials of SHCC materials. A comprehensive multiscale experimental investigation is presented from single fiber/matrix bonds (microscale) to uniaxial tensile tests on miniature notched specimens (mesoscale) and unnotched specimens (macroscale). This investigation aims to elucidate the mechanisms by which the micromechanical criteria established by the SHCC constitutive law are met and strain-hardening is achieved with highly compliant PP fibers, and the profound difference that exists with SHCC incorporating PE fibers.

2. Materials

2.1. Raw constituents for SHLC^4 mixtures

In this study, three matrices were examined: LC^3-50, LC^3-35, and LC^3-25, featuring a PC content of 50 %, 35 %, and 25 % by weight of the binder, respectively. The subsequent details are in the context of strain-hardening limestone calcined clay cementitious composites, abbreviated as "*SHLC*^{4}". Portland cement, CEM I 52.5 R-SR3/NA, was sourced from Holcim GmbH, Lägerdorf, Germany. It is a high-strength, rapidly

hardening, sulfate-resistant cement with C_3A content of the clinker ≤3 % as per EN 197-1 standard [52]. A special thermally treated clay, characterized by its low kaolinite content (limited to 25 % by weight), was obtained from Liapor GmbH & Co. KG., in Hallerndorf, Germany. Under the tradename "*Saxodol 90 LE*", a limestone powder and high-purity gypsum were procured from sh Minerals GmbH in Heidenheim/Brenz and Grüssing GmbH, respectively, both located in Germany. The chemical and mineralogical composition of binder materials is listed in Tables 1 and 2, respectively.

To produce fine-grained mortars, fine quartz sand was added to the binders as inert aggregate, characterized by particle sizes ranging from 60 to 200 μm, supplied by Strobel Quarzsand, Germany. For achieving good fiber dispersion and maintaining the fresh mixture's workability, a viscosity modifying agent (VMA), Unterwasser-Compound 100 from Sika®, Germany, and a polycarboxylate (PCE)-based superplasticizer, MasterGlenium ACE 460, provided by Master Builders Solutions, Germany, were incorporated into the mix designs. Fig. 1 showcases the particle size distributions of the binder and filler fines used in formulating different SHLC^4 mixtures, measured using a laser diffraction particle size analyzer (LS I3 320, Beckman Coulter). Table 3 lists the median grain sizes, densities (ρ), and specific surface areas (*SSA*).

This study examines two types of dispersed fiber reinforcement: ultra-high molecular weight polyethylene (UHMWPE, referred to as "*PE*"), which serves as the reference, and standard polypropylene (PP) as an economical and more viable substitute for PE. Both PE and PP are polyolefins and are characterized by a non-polar nature [53]. As a result, PE and PP fibers inherently possess hydrophobic surfaces, implying that they can only form mechanical bonds and do not interfere with the hydration mechanism in cementitious systems [54]. Furthermore, these fibers are known for their exceptional chemical stability in both acidic and alkaline environments – the latter is crucial as it is typical in cementitious systems. Table 4 reports a summary of their physical and mechanical properties as per the manufacturers' datasheets [55,56].

2.2. Mixture design of SHLC^4

The following measures were taken in the design of matrices suitable for compliant PP fibers to achieve strain-hardening behavior: (i) high volume substitutions of limestone and calcined clay, *i.e.,* to reduce the cement clinker content, and a high water/binder ratio of 0.4 to further increase the dilutive effects – both these measures contributed to a less dense microstructure of the matrix, thereby leading to a high number of internal flaws (high porosity), which facilitates crack initiation and propagation; (ii) a higher volume fraction of PP fibers in the SHLC^4 compositions, *i.e.*, 2.5 %, as opposed to 2 % for the reference PE fibers, to compensate for loss in bridging capacity due to the low intrinsic tensile strength of PP; (iii) a low sand/binder ratio of 0.23, to reduce the fracture toughness of the matrices to allow for easier crack propagation [57]; and (iv) a sufficiently high aspect ratio (L/D) of the fibers – *cf.* Table 4 – to allow sufficient bonded lengths in the crack flanks for improved crack-bridging capabilities.

Table 5 presents the mixture compositions (kg/m^3) of the three matrices under investigation. In these matrices, the weight ratio of LS to CC was kept at 1:2, while gypsum was added in 3 wt% of the binder for proper sulfation [58]. The superplasticizer was added at a concentration of 0.68, 1.23, and 2.10 wt% of PC in SHLC^4-50, SHLC^4-35, and SHLC^4-25, respectively, to enhance the fresh mix workability and improve fiber dispersion. As illustrated in Fig. 2, a representative example demonstrates the workability of SHLC^4-25-PP. Additionally, the figure presents the mean spread diameter measurements obtained after 15 strokes using the Hägermann flow table test method. Across the various SHLC^4 samples, no instances of fiber agglomeration or water bleeding were observed, indicating a homogeneous fiber dispersion and stable mixture consistency.

Table 1
Chemical composition (wt.%) of the raw binder ingredients as determined by energy dispersive X-ray (EDX) analysis.

Chemical oxides	Portland cement	Calcined clay	Limestone	Gypsum
SiO_2	16.1	47.4	7.3	0.9
Al_2O_3	3.5	24.8	1.9	3.3
Fe_2O_3	4.3	8.9	0.8	0.1
CaO	71.6	8.6	75.4	43.2
MgO	1.1	2.8	14.1	1.1
SO_3	3.4	2.2	–	51.1
P_2O_5	0.2	–	0.2	0.1
K_2O	0.5	3.6	0.4	0.1
Na_2O	–	0.4	0.5	–
TiO_2	0.3	1.3	–	–

3. Experimental program

3.1. Single fiber tension test

The fiber tensile tests were performed to verify the tensile strength, tensile modulus, and elongation at break for PP and PE fibers. The experimental design encompassed a total of eight replicates for each fiber type. Prior to the execution of the tests, the diameter of at least 20 fibers of each type was measured using electron scanning electron microscopy (ESEM). These nominal diameter values were averaged and used to evaluate the tensile strength of the fibers tested.

To perform the tests, the fibers were attached to paper frames with a 6 mm opening in the center that served as the free length of the fiber. Cyanoacrylate adhesive anchored the fibers to the paper frame at the upper and lower ends. The test was conducted on a Zwick 1445 testing machine with a 10 N load cell under a controlled displacement rate (0.05 mm/s). The paper frames were inserted into the two mechanical clamps and tightened with screws. Afterward, the lateral sides of the paper clamps were cut in correspondence with the free fiber length portion, and the test was initiated. Fiber elongation was equated to the displacement of the machine's crosshead. Readers are referred elsewhere for a detailed schematic view of the test setup and single fiber tensile test specimens [59].

3.2. Flexure and compression test on SHLC^4 samples

Prismatic beam-like specimens of 40 × 40 mm^2 cross-section and 160 mm length were selected to evaluate the flexural performance of the composites investigated under three-point bending test. Following the flexural test, 40 mm cubes were extracted from undamaged prismatic beams for compression tests.

According to the recipes listed in Table 5, the mixtures were prepared according to the protocol explained by Wang et al. [30]. The molds were filled layer-by-layer to align the fibers in the longitudinal direction of the specimen, which is particularly important for the bending and uniaxial tension tests. Immediately after casting, the specimens were covered with a metal plate and cured in the molds for 24 h. Afterward, they were de-molded and further cured in a sealed condition in a climatic chamber at a constant temperature (20 °C) for another 27 days. An EU 20 hydraulic testing machine, manufactured in Germany, was employed to execute the bending tests, which were conducted with a net span of 100 mm under controlled displacement rate of 0.05 mm/s. Three beams were tested for assessing flexural performance. The compression test was conducted with the same machine in a load-controlled configuration (2.4 kN/s) on six cubes in accordance with DIN EN 196-1 [60].

3.3. Fiber/matrix interfacial characteristics

Single fiber pull-out (SFPO) test was performed to quantify the fiber–matrix interaction. Single fibers were embedded in different LC^3-

Table 2
The mineral composition of raw binder materials determined by XRD-Rietveld analysis.

Portland cement		Calcined clay		Limestone		Gypsum	
Minerals	**Wt. [%]**	**Minerals**	**Wt. [%]**	**Minerals**	**Wt. [%]**	**Minerals**	**Wt. [%]**
C_3S	57.4	Quartz	18.8	Calcite	54	Gypsum	91
C_2S	19.3	Mica	6.6	Dolomite	44	Anhydrite	6
C_3A	2.7	Feldspar	4.9	Others	2	Calcite	3
C_4AF	13.6	Anhydrite	1.8	–	–	–	–
Calcite	1.8	Calcite	1.8	–	–	–	–
Gypsum	1.7	C_3A	0.4	–	–	–	–
Bassanite	3.5	Amorphous	65.7	–	–	–	–

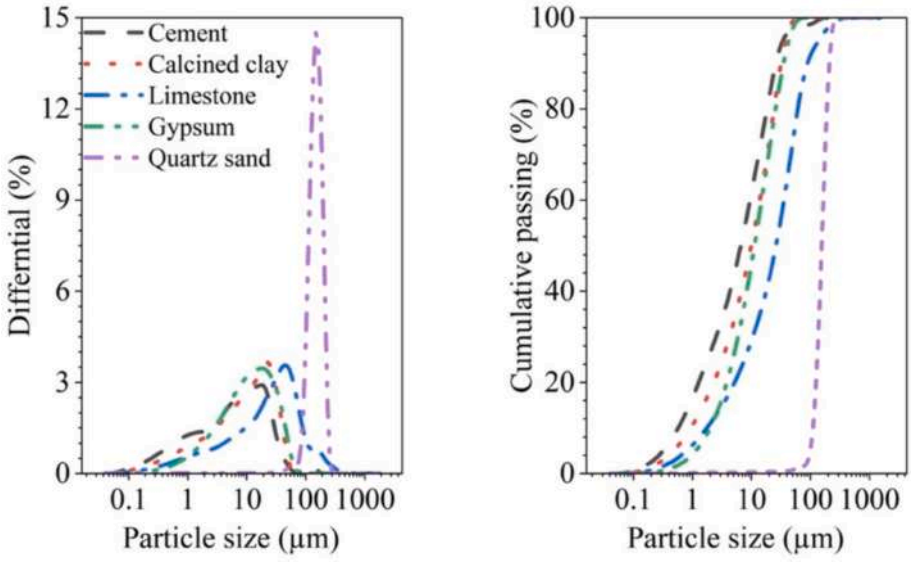

Fig. 1. Particle size distribution of raw ingredients.

Table 3
Physical properties of the binder and filler fines.

Properties	Portland cement	Calcined clay	Limestone	Gypsum	Sand
Median grain size [μm]	7.1	9.9	26.1	11.3	155.8
Density (ρ) [kg/m^3]	3150	2600	2770	2380	2750
Specific surface area (SSA) [m^2/g]	1.3	7.6	1.7	1.8	0.02

Table 4
Physical, mechanical, and geometrical properties of PE and PP fibers, according to the manufacturers [55,56].

Fiber type	PE	PP
Manufacturer, country	DSM, the Netherlands	IFG Asota, Austria
Brand name	Dyneema SK78	Asota AFC/MCP
Length (L in mm)	12	12
Diameter (D in μm)	18	18
Aspect ratio (L/D)	666.7	666.7
Tensile strength (MPa)	3400	≥ 400
Young's modulus (GPa)	~ 120	–
Elongation at break (%)	3.5	≤ 80
Density (g/cm^3)	0.97	0.91

based matrices. Two specially designed devices at the Leibniz-Institut für Polymerforschung Dresden e.V. [61,62] were used to accurately embed the fiber and perform the SFPO tests. The test setup is illustrated in Fig. 3.

Table 5
SHLC[4] mixture compositions, in kg/m^3.

Raw ingredients	SHLC[4]-50	SHLC[4]-35	SHLC[4]-25
Cement	586	405	287
Limestone	188	246	283
Calcined clay	376	491	565
Gypsum	18	12	9
Quartz sand	263	260	257
Fibers	20[a] / 23[b]	20[a] / 23[b]	20[a] / 23[b]
Water	468	463	459
Superplasticizer	4	5	6
VMA	4	4	4

[a] 2% volume fraction of PE fibers.
[b] 2.5% volume fraction of PP fibers.

First, the fibers were separated into individual filaments and cut to a length of about 20 mm. The premixed dry components of the matrices were mixed with a previously prepared water/superplasticizer solution in a high-speed mixer for 120 s at 2500 rpm. Approximately 3 ml of cementitious matrices were prepared per batch and used for embedding purposes for 10–15 min to avoid effects caused by the onset of the hardening process. The mixture was then transferred to a cylindrical brass specimen holder with an internal diameter of 2.6 mm. The single fiber was then embedded under computer control at a constant rate of 200 μm/s^{-1} to a total embedment length of approximately 2000 μm (2 mm). After 5–10 min, the specimen holder with the embedded fiber was transferred to a water-filled desiccator to maintain a humid atmosphere for a total curing time of 28 days.

To perform the SFPO, 14–21 specimens were tested for each fiber/

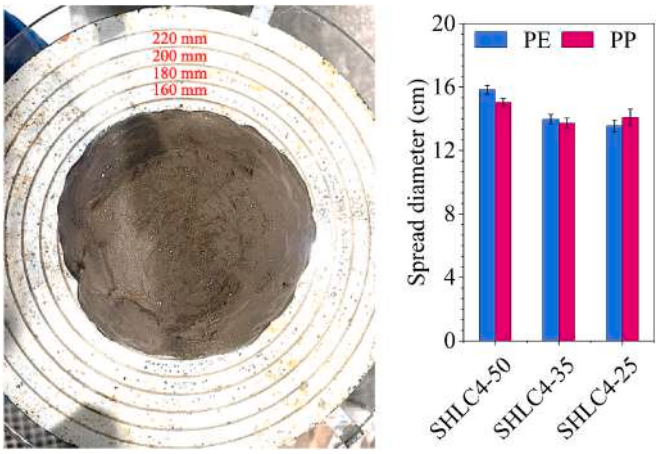

Fig. 2. An example of SHLC^4-25-PP spread diameter (left) and the average spread diameter of all SHLC^4 compositions under investigation after 15 strokes (right), as determined by the Hägermann flow table test method.

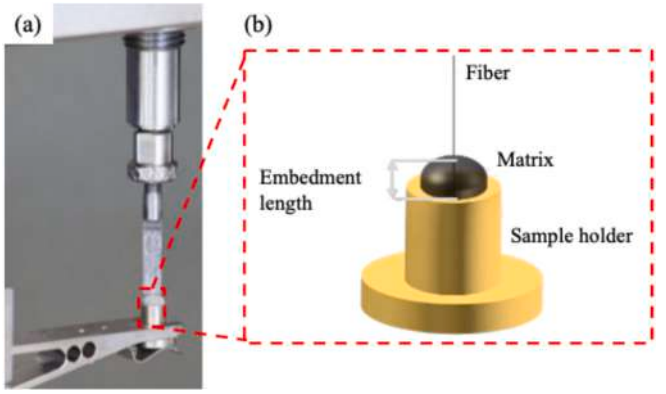

Fig. 3. (a) SFPO specimen with fixed single fiber to the sample holder, and (b) schematic SFPO model, adapted from [62].

matrix combination. A cyanoacrylate adhesive was used to fix the free single-fiber end to the specimen holder. Quasi-static SFPO was performed at a rate of 0.001 mm/s. The interfacial bond properties, *i.e.*, frictional bond (τ) and pull-out work (*W*), were then determined from the force–displacement curves obtained using Eqs. (1) and (2).

$$\tau = \frac{P_B}{\pi d_f L_e} \tag{1}$$

$$W_f = \int_0^{\delta(P_f)} P d\delta \tag{2}$$

where P_B corresponds to the force at the onset of the pull-out phase; d_f is the fiber diameter (18 μm); L_e is the embedded length of the fiber (2 mm); and $\delta(P_f)$ is the slip at the point of interest, *e.g.*, the subscript "*f*" is 1.0 for 1 mm slip value.

3.4. SHCC constitutive law – Bridging stress vs. single crack opening displacement

Miniature specimens were cast and subjected to tensile loads to assess the bridging stress of the fibers as a function of the notch opening. This relationship plays a key role in the determination of the micromechanical criteria for strain hardening in fiber reinforced composites. These specimens were cut from thin dumbbell-shaped plates fabricated using a special mold designed for such dimensions: 100 mm gauge length, 40 mm width, and 3 mm thickness in the gauge region. The detailed production process for such specimens is highlighted elsewhere [63–65]. The SHLC^4 compositions were cast into the molds, and the desired small thickness was achieved by pressing an upper mold element into the freshly poured mixture, pushing it in a longitudinal direction toward the mold ends while simultaneously aligning the fibers in the same direction. After 24 h, the specimens were de-molded, followed by a curing protocol matching flexure and compression specimens.

One day before testing, the excess material at the specimen edges was cut away, leaving only the gauge region, from which thin longitudinal strips were cut to produce miniature specimens measuring 50 mm long with cross-sectional dimensions of 10 mm × 2.5 mm. Then, using a 1.5 mm thick circular saw, 2 mm deep notches were made in the center of the specimen's length, resulting in a 40 % reduction in cross-section to ensure the initiation and localization of a single crack in the notched region during the tensile test.

The uniaxial tension test was performed in a Zwickline Z2.5 testing machine with a 2.5 kN load cell under a controlled displacement rate (0.05 mm/s). A minimum of four specimens were tested for each fiber/matrix pairing. The specimens were mechanically clamped in special steel clamps, with clamping areas of 15 × 10 mm^2. A torque-controlled screwdriver was used to ensure uniform clamping pressure and prevent specimen slippage. The force and displacement signals were recorded directly from the machine's load sensor and crosshead movement to assess fiber bridging stress and crack opening displacements, respectively. Due to very small size of the specimens, it was not possible to attach more accurate external displacement measurement devices, such as LVDTs, and this may slightly overestimate the measured displacements. Fig. 4 illustrates the geometrical details of miniature specimens and testing setup details.

3.5. Uniaxial tensile test

For uniaxial tensile tests performed on SHLC^4, dumbbell-shaped specimens were employed. The specimens have a total length of 250 mm and a gauge length of 100 mm. The cross-section varies smoothly from 24 mm × 40 mm along the gauge length to 40 mm × 40 mm at the clamping area. Further graphical details of the specimens are presented in Fig. 5. These specimens were cast and cured like those of the prismatic samples used in the compression and flexure testing. Additionally, the samples were marked with a fine speckle pattern of black dots against a white background to aid digital image correlation (DIC) for in-situ crack analysis.

The tests were performed on an Instron 8802 testing machine using a set of in-house designed mechanical clamps to hold the specimens in place, offering rigid boundary conditions. A minimum of four replicates were executed for each combination of fiber and matrix under investigation. DIC analysis was performed using a high-intensity light source and stereo camera setup provided by Carl Zeiss GOM Metrology GmbH. The cameras were synchronized with the Instron load sensor, so data recording automatically commenced when the 500 N preload threshold was breached. Operating at a frequency of 2 Hz, the images were recorded with real-time force and machine displacement readings, set at identical sampling rates, in the Aramis professional software (Carl Zeiss GOM Metrology GmbH) for analysis.

The software employed two virtual strain gauges affixed to both ends of the specimen within the gauge length. It enabled precise computation of axial strains by measuring their relative deformations across all frames captured during the tests and referenced to the initial image. Furthermore, crack widths were calculated by applying similar virtual calipers to each crack that surfaced within the gauge area during the experiment and evaluating their relative openings. Finally, the number of cracks was manually counted at the stage corresponding to the tensile strength.

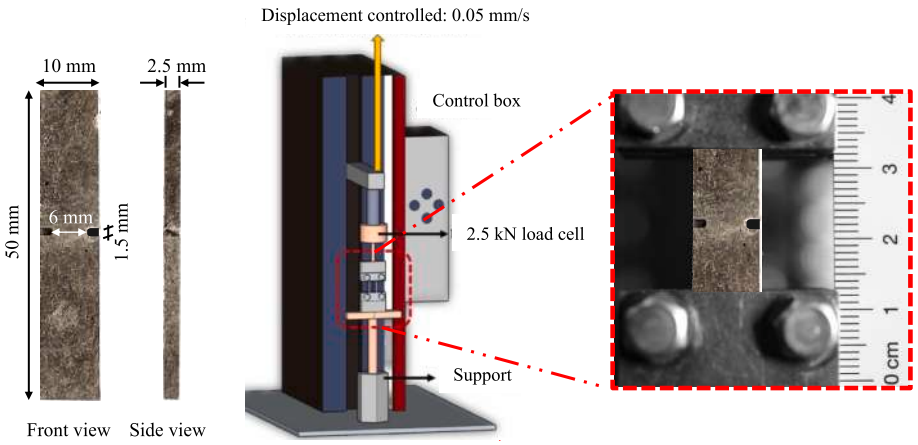

Fig. 4. Miniature notched specimen's geometrical details and testing setup.

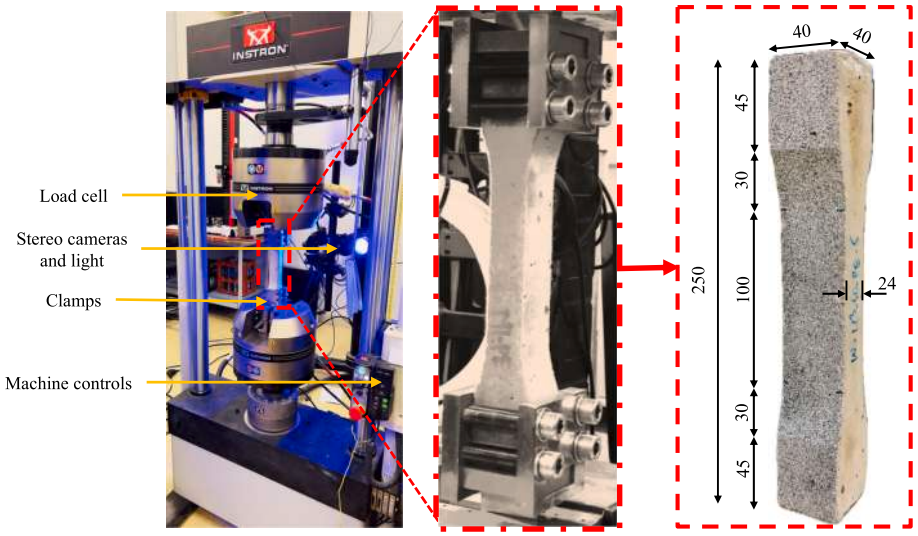

Fig. 5. Dumbbell specimen's geometrical details and uniaxial tensile testing scheme.

4. Results and discussion

4.1. Single fiber tension tests

Fig. 6(a) shows the morphology of the two fibers as observed by ESEM. The analysis revealed that the reference PE fibers are characterized by longitudinal grooves distributed along the entire surface. In contrast, the surface of the PP fiber appeared to be smoother, suggesting different degrees of mechanical bond when embedded in cementitious matrices. The ESEM analysis was further extended to measure the diameter of the adopted fibers, which was found to be 18 μm, in agreement with the manufacturer's specifications. The measured diameters were employed to assess the cross-sectional areas of the fibers and subsequently determine their tensile strength. Fig. 6(b) plots the envelopes of single fiber tensile stress *vs.* strain curves of PE and PP fibers, while the key properties from this test, *i.e.*, tensile strength, fiber elongation at break, and tensile modulus, are listed in Table 6.

Mechanical characterization revealed that PP fibers exhibited 86.4 % and 93.2 % reduced tensile strength and modulus, respectively, and 437.5 % greater elongation at break than PE fibers, substantiating the low tensile strength and remarkable compliance of the PP fibers relative to those of PE fibers. The manufacturing process of these fibers has a significant impact on their mechanical performance. Indeed, PP fibers are typically manufactured using a faster and less expensive melt-spinning process, as opposed to the complex gel-spinning process employed to produce UHMWPE (PE) fibers [62,66,67]. The gel-spinning process is adapted explicitly for UHMWPE due to the long polyethylene chains (high molecular weight) to achieve a high degree of molecular orientation. This results in the generation of fibrils that are visible at the fiber surface and a very high degree of crystallinity. As a result of this process, the surface of these UHMWPE fibers is usually rougher compared to PP fibers, and the strength and stiffness of UHMWPE fibers are high, rendering them one of the strongest polymer fibers currently available on the market [37,66,68].

4.2. Flexure and compression tests

Before undertaking the scale-linking investigations on SHLC^4 in the forthcoming sections, a series of 3-point bending and uniaxial compression tests were conducted to establish a general performance benchmark. The results of these tests are presented in Fig. 7.

All SHLC^4 exhibited deflection-hardening (not shown here), analogous to strain-hardening in uniaxial tensile tests, associated with multiple cracking due to fulfillment of the *strength* and *energy criteria* (discussed in Section 4.5). SHLC^4-50-PE exhibited the highest flexural strength, which gradually declined with increasing binder dilution with SCMs. On the contrary, all PP-reinforced SHLC^4 maintained flexural strength around 12–14 MPa, indicating that the matrix strength had no

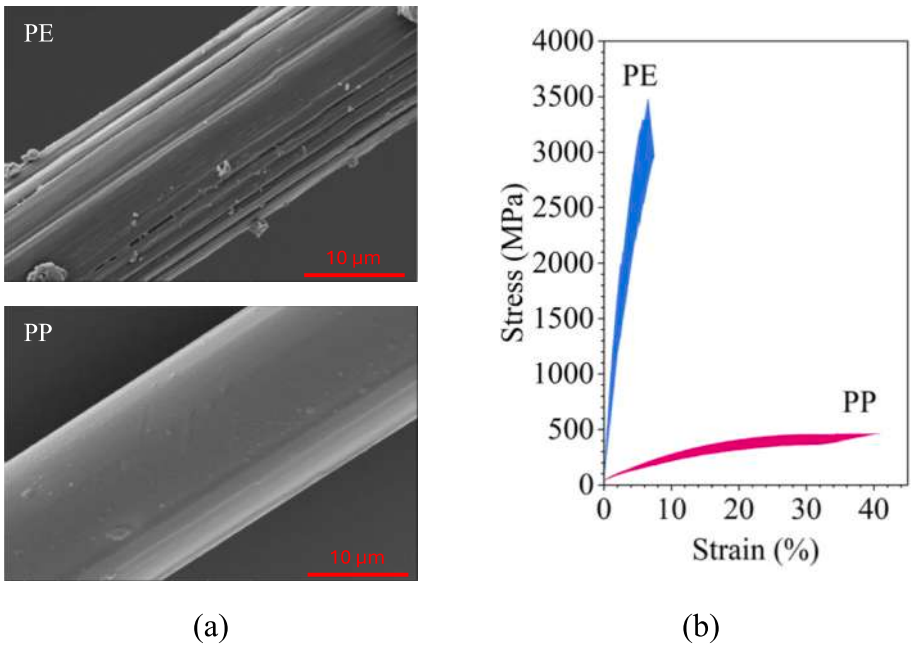

Fig. 6. (a) Morphology of PE and PP fibers, and (b) their tensile stress *vs.* strain curves.

Table 6
Average tensile properties of PE and PP fibers; standard deviations are given in parentheses.

Fiber type	Tensile strength [MPa]	Fiber elongation at break [%]	Tensile Modulus [GPa]
PE	3192.1 (164.7)	6.4 (0.7)	88.0 (29.0)
PP	434.6 (38.0)	34.4 (3.2)	6.0 (1.2)

significant impact on this property. In contrast, when the same matrix formulation was employed, the compressive strength of PP-based SHLC[4] were marginally superior to that of PE-based SHLC[4]. Nevertheless, all the composites exhibited 28-day compressive strength between 25–40 MPa. From a practical point of view, this strength range is well within, or even slightly exceeding, the currently employed concrete strength range of 25–35 MPa for structural applications [69].

These strength metrics, particularly compressive strengths, can be employed to gain insights into the strain-hardening potential of a specific fiber and matrix pairing. For example, given that the tensile strength of PP fibers is relatively low, the high-strength matrices – specifically, HS-SHCC (M2), which encompasses a compressive strength of 130–140 MPa – that have been previously investigated in references [70,71], would fail to meet the strength criterion that is decisive for strain-hardening behavior. A similar hypothesis is proposed regarding the previously investigated LC[3] matrix (*cf.* Ahmed *et al.* [29]) featuring a compressive strength of 80 MPa. Pairing matrices with high compressive strength with high-performance fibers is much more effective regarding the price-to-performance ratio. However, this approach limits the sustainability profile of SHCC. Therefore, this strategy should only be employed where specific high performance is crucial. The forthcoming sections experimentally verify this notion by pairing various matrices encompassing different strengths with different fibers.

4.3. Fiber/matrix interfacial characteristics

Fig. 8 shows the force *vs.* slip curves from which the fiber/matrix interface properties of LC[3]-50, LC[3]-35, and LC[3]-25 matrices embedding PE and PP fibers were ascertained. In particular, pull-out test curves for PE fibers are shown in blue in inlets a-c, and pull-out test curves for PP fibers are shown in magenta in inlets d-f, in both cases, with matrices moving from the lowest to the highest PC replacement level.

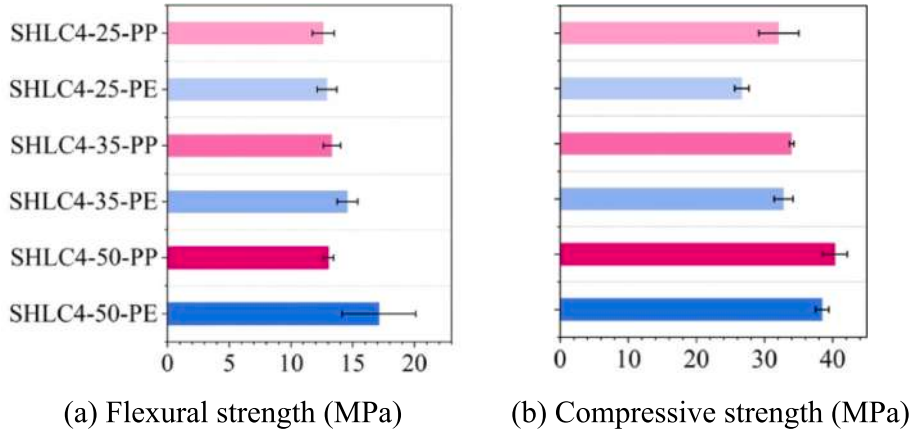

Fig. 7. (a) Flexural strength and (b) compressive strengths of various SHLC[4] under investigation.

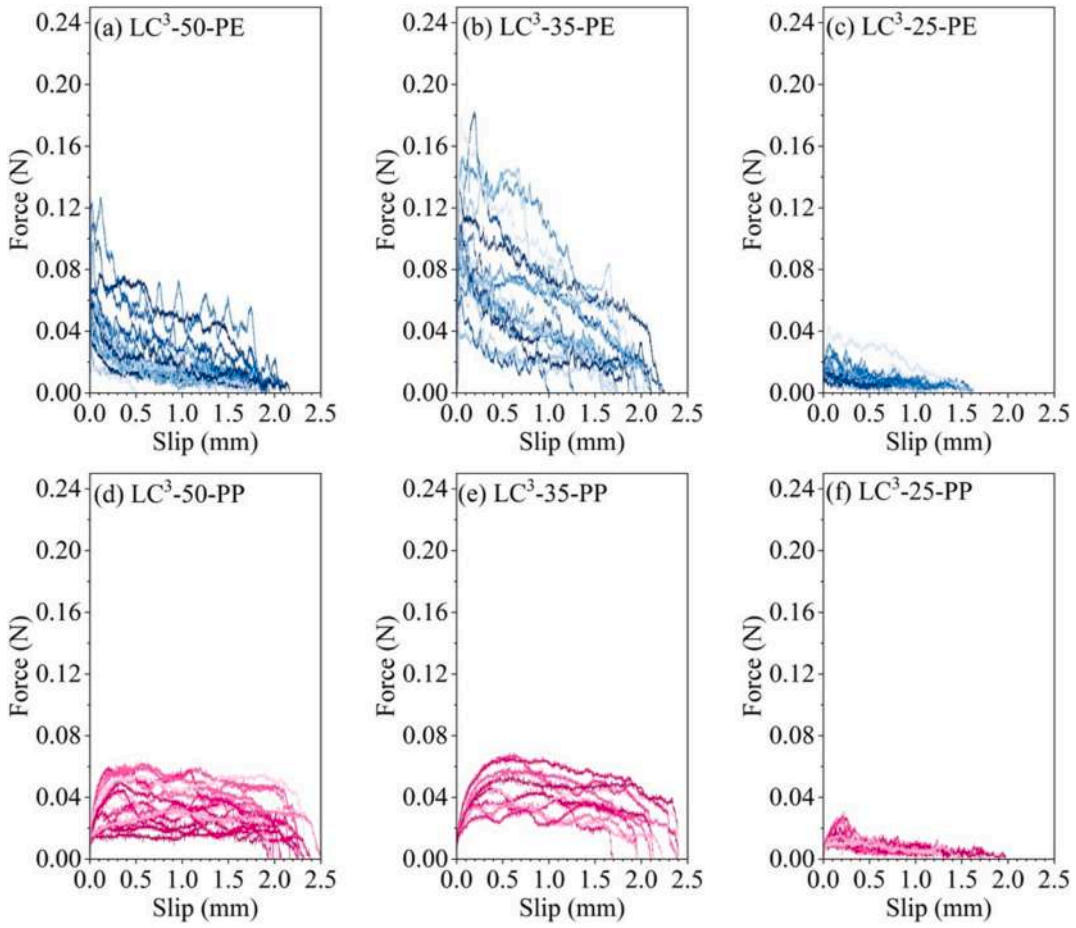

Fig. 8. Force *vs.* slip curves from single fiber pull-out tests for each matrix and fiber type variation.

4.3.1. Debonding phase

Although PP and PE fibers were embedded in the same matrix, the pre-peak pull-out behavior (debonding phase) exhibited distinct characteristics, indicating that the fiber type substantially influences the debonding phase. In moderately diluted matrices, such as LC^3-50 and LC^3-35 mortars, the embedded PP fibers exhibited a 28.6 % and 54.5 % reduction in peak force (debonding force), respectively, see Table 7, and a shallower rise to peak force than their PE counterparts. However, in highly diluted LC^3-25 matrices, the two fiber types exhibited equal debonding forces. This phenomenon can be elucidated through applying principles based on solid mechanics. The fiber pull-out from the matrix can be conceptualized as a system in which the stiffness of the two components, namely the fiber and the matrix, act in series. (*cf.* Fig. 9). The ascending slope in the debonding phase represents the system's equivalent stiffness (K_{Eq}). Thus, when the pullout force is applied, both the fiber stiffness (K_f) and bond stiffness (K_b) (related to the matrix stiffness), work in conjunction to distribute the load in the system and define the force-slip response achieved. The relationship that computes the K_{Eq} for a system in series configuration is also mentioned in Fig. 9. As the matrix becomes more dilute, for example, from LC^3-50 to LC^3-25, the bond stiffness decreases, resulting in a decrease in K_{Eq}. Likewise, if the fiber is compliant, as in the case of PP, the K_{Eq} also decreases. Consequently, the debonding phase also exhibits either compliant or stiff behavior when compliant or stiff fibers are pulled out of the same matrix.

Table 7
Summary of bond properties results attained from single fiber pull-out test results; the standard deviation is given in parentheses.

Bond properties	LC^3-50		LC^3-35		LC^3-25	
	PE	PP	PE	PP	PE	PP
Maximum debonding force [N]	0.07 (0.03)	0.05 (0.01)	0.11 (0.04)	0.05 (0.01)	0.02 (0.01)	0.02 (0.01)
Frictional bond strength – τ [MPa]	0.50 (0.24)	0.34* (0.15)	0.96 (0.35)	0.42* (0.11)	0.16 (0.07)	0.13* (0.04)
Pull-out work @ 1 mm slip – $W_{1.0}$ [Nm × 10^{-6}]	32.96 (21.49)	34.19 (13.69)	77.85 (33.47)	40.99 (8.95)	8.63 (5.54)	9.59 (3.95)
Total pull-out work– W_T [Nm × 10^{-6}]	47.28 (34.17)	68.17 (28.37)	111.57 (53.62)	79.89 (23.73)	11.69 (6.80)	13.62 (6.58)

* Eq. (1) doesn't provide accurate bond strength for soft polymeric fibers embedded in hard concrete-like matrices. It mainly serves here as a qualitative parameter.

To illustrate this phenomenon, consider the pre-peak trend in pull-out curves, emphasizing different fiber and matrix pairings (Fig. 10). For instance, the incorporation of compliant PP fibers within the relatively stiff LC^3-50 matrix inherently induces a pronounced stiffness mismatch at the fiber/matrix interface, reducing overall K_{Eq}. Consequently, when subjected to fiber pull-out, the load transfer from the PP fiber to the fiber–matrix interface is gradual, accompanied by significant fiber elongation and diameter shrinkage due to Poisson's effect. In contrast, the load transfer is very abrupt when relatively stiffer PE fibers are incorporated into relatively stiff LC^3-50, naturally increases the equivalent stiffness of the system, K_{Eq}.

To further elucidate the concept, it is imperative to consider an alternative scenario, namely, relatively stiff PE in a relatively compliant

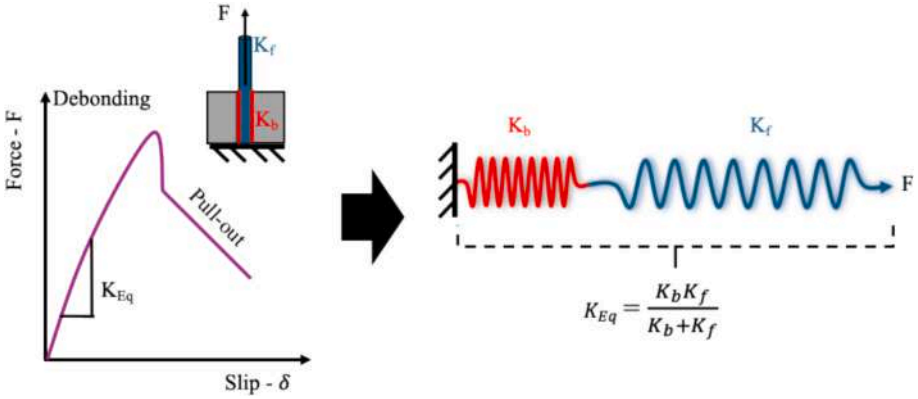

Fig. 9. Schematic of a simple engineering model for a single fiber pull-out test.

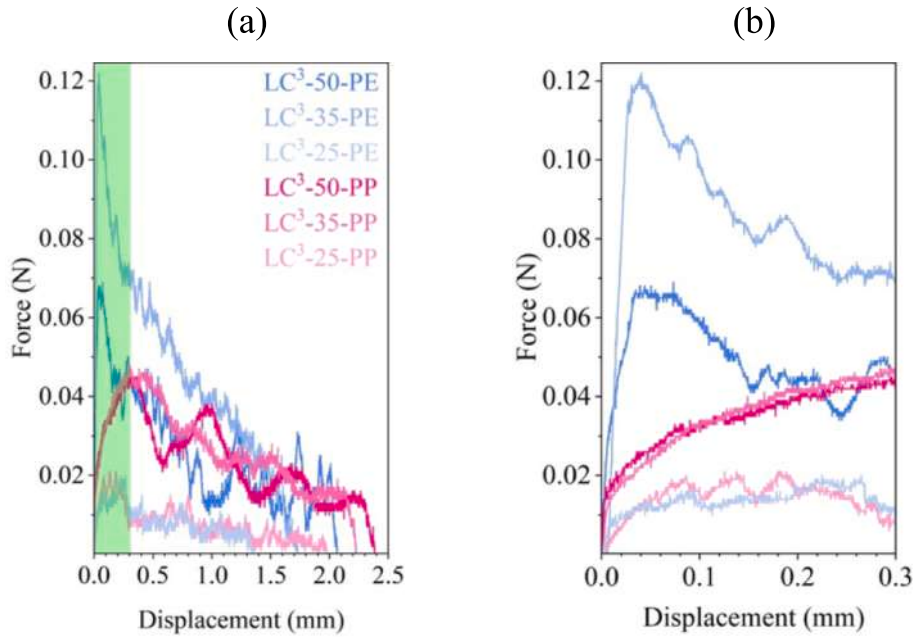

Fig. 10. (a) Representative force *vs.* displacement curves from single fiber pull-out tests, and (b) zoomed view for visualizing the debonding phase.

LC^3-25 matrix. In this configuration, the discrepancy between the stiffness of the fibers and that of the matrix is once again more pronounced, culminating in a substantial reduction in the K_{Eq} due to the reduced matrix stiffness. This reduction in matrix stiffness enables the extraction of PE fibers with minimal deformation. As a consequence, the pre-peak pull-out curves show that LC^3-50-PE and LC^3-35-PE exhibited high K_{Eq} (steeper slope in debonding region) whereas LC^3-25-PE and all LC^3 matrix variants incorporating PP exhibited lower K_{Eq} (shallower slope in debonding region).

It is noteworthy that when PE and PP fibers were integrated into the LC^3-35 matrix, no reduction in the debonding force in relation to the denser LC^3-50 matrix was observed (*cf.* Table 7), despite the lower clinker factor and higher dilutive effect in the former matrix. One plausible explanation for this unexpected response lies in the physical and chemical nature of the LC^3-35 matrix, particularly in the vicinity of the fiber/matrix interface. Physically, LC^3-35 exhibits slightly reduced compaction and elevated porosity [58], with a greater concentration of unreacted calcined clay and limestone. These elements contribute to enhanced resistance to fiber pull-out due to their irregular morphology. The authors previously demonstrated this phenomenon when two distinct high-volume substitution levels of CC and LS with PC in SHCC were investigated [51]. Despite a notable decline in compressive strength as the proportion of clinker replacement increased, the peak fiber bridging capacity remained unaltered in both SHCC.

Chemically, the presence of a greater quantity of calcined clay and limestone in LC^3-35 than in LC^3-50 was observed to result in the formation of a greater number of carboaluminate phases (AFm-Mc), and a relatively higher degree of pozzolanic reaction in the former over the course of 7 to 28 days of curing [58]. This was primarily due to the filler effect of added SCMs [72,73]. However, it can also be reasonably inferred that as the proportion of PC replaced increases, the excess SCMs near the fiber and matrix will no longer impart these positive physicochemical aspects responsible for the matrix's microstructure build-up. Indeed, there is a threshold level of SCM substitution beyond which the microstructure becomes so diluted that there are insufficient hydrates to yield sufficient matrix strength and maintain the bonding of unreacted SCM particles to the matrix. Consequently, the LC^3-25 formulation has been found to diminish the bonding characteristics of the fiber/matrix markedly.

This further highlights the importance of a more careful SHCC design, one that considers performance together with sustainability and financial implications. For instance, these results above clearly demonstrated a mismatch in terms of interfacial properties, particularly debonding forces, for PP fibers compared to PE counterparts, underlying

a lack of crack-bridging capacity. Accordingly, for this study, it was deemed necessary to compensate for this gap by increasing the volume fraction of the PP fibers to 2.5 % (compared to the reference dosage of 2 %). This additional volume fraction of PP fibers has minimal impact on the processability of the fresh LC^3 blends (see Fig. 2) but was essential to meet the two critical micromechanical criteria for strain hardening behavior – *strength* and *energy criteria* – presented in Section 4.4.

4.3.2. Pull-out phase

As for the post-peak profile of the pull-out curves for PE fibers in different LC^3 matrices, a slip-independent trend was observed. That is to say, there was an almost linear decay of the pull-out force with increasing slip (see Fig. 8). This response is characteristic of highly stiff and hydrophobic fibers, such as PE [63,74,75]. Conversely, in the case of highly compliant PP fibers, the shape of the pull-out curves indicated either slip-hardening or slip-independent behavior with a relatively shallower decay. This phenomenon can be attributed to the significant plastic deformation of the PP fibers that initiates even at low applied stress levels (*cf.* Fig. 6(b)), which effectively counteracts the decrease in pull-out force as the fibers slip from the matrix.

The interfacial frictional bond strength was estimated using Eq. (1) for PP and PE fibers. It should be noted, however, that this equation has inherent limitations when considering soft polymer fibers, as this equation doesn't account for fiber elongation (*e.g.,* plastic deformation) and, Poisson's effect during pullout from hard concrete-like matrices [76]. In such cases, the pull-out work (W), as defined by Eq. (2), can be better alternative metric. W represents the energy dissipation during debonding and fiber pull-out from the matrix. The calculations were performed at two distinct slip values, *i.e.*, 1 mm ($W_{1.0}$) and complete pull-out work (W_T). The large scatter in the W_T values is due to the experimental uncertainty in the total embedment length between different specimens. Nevertheless, it remains a robust metric for pinpointing the increasing or decreasing trend because the crack-bridging fibers in SHCC also have varying embedment lengths.

For a direct comparison, $W_{1.0}$ was evaluated at a fixed slip value of 1 mm to assess the energy dissipation during fiber pull-out. Although LC^3-50-PP demonstrate lower debonding force and frictional bond strength compared to LC^3-50-PE, its $W_{1.0}$ remained comparable. This suggests that, despite the contrasting inherent mechanical properties of PP and PE fibers, both fiber types can provide sufficient fiber-bridging capacity when embedded in a similar matrix. The ability of PP fibers to undergo large plastic deformations compensates for their lower interfacial bond strength, resulting in comparable energy dissipation during pull-out.

In the LC^3-35 matrix, PP-based samples exhibited a 47 % lower $W_{1.0}$ than their PE counterparts. This was primarily due to the higher debonding force of PE fibers, which required greater energy to initiate pull-out. Likewise, LC^3-35-PP outperformed LC^3-50-PP by 20 % in $W_{1.0}$, suggesting that the LC^3-35 matrix offers better interfacial bond strength and increased energy dissipation before complete fiber extraction. However, in a highly diluted matrix, such as LC^3-25, the values of $W_{1.0}$ were comparable across fiber types. In this case, the weak matrix led to insufficient fiber anchorage, allowing easier pull-out with limited fiber elongation.

4.4. SHCC constitutive law – Bridging stress vs. Single crack opening displacement

This section presents the results of the experimental assessment of the SHCC constitutive law ($\sigma - \delta$), *i.e.*, fiber bridging stress *vs.* crack opening displacement (COD), based on uniaxial tensile tests on miniature notched specimens. In order to achieve strain-hardening behavior with specific fiber and matrix types, two well-known criteria, driven by micromechanical laws, *i.e.*, the "*strength criterion*" and the "*energy criterion*", must be met [1,4,77]. The *strength criterion* stipulates that the fiber bridging stress (σ_b) must consistently exceed the matrix cracking stress (σ_m) in each crack plane, that is to say, $\sigma_b \geq \sigma_m$. This guarantees that the bridging fibers can take over and transfer the applied load deeper into the intact matrix portions in the event of a matrix integrity loss in correspondence with a crack plane. As long as the condition above holds true, multiple cracks will continue to form. The larger the mismatch between σ_m and σ_b, the more pronounced the strain-hardening behavior is expected to be. A pseudo-strain hardening (*PSH*) performance index (Eq. (3)) is usually employed to assess these margins on a quantitative basis [78].

$$PSH_{strength} = \frac{\sigma_b}{\sigma_m} \tag{3}$$

The stress (σ) values are obtained by dividing the tensile load by the cross-sectional area of the notch. σ_m is the stress level at the first inflection point and σ_b is the peak stress in the fiber bridging stress *vs*. COD curves in Fig. 11.

The *energy criterion* serves to regulate the steady-state crack propagation (flat crack, *i.e.,* constant crack tip opening displacement) and to control whether the bridging fibers undergo pull-out or rupture. The fulfilment condition of the energy criterion is that the energy contribution of the bridging fibers (complementary energy – J_b') remain markedly higher than the toughness of the matrix at the crack tip (J_{tip}): $J_b' \geq J_{tip}$. These energy contributions from the crack tip toughness and bridging fibers can be evaluated by J-integral method [79] using Eqs. (4) and (5), respectively. Consequently for the *energy criterion*, a large margin between J_{tip} and J_b' is required to ensure good strain hardening, which can be estimated quantitatively using a second *PSH* performance index, as defined in Eq. (6).

$$J_{tip} = \sigma_m \delta_m - \int_0^{\delta_m} \sigma(\delta) d\delta \tag{4}$$

$$J_b' \equiv \sigma_b \delta_b - \int_0^{\delta_b} \sigma(\delta) d\delta \tag{5}$$

$$PSH_{energy} = \frac{J_b'}{J_{tip}} \tag{6}$$

Table 8 presents the key mechanical parameters derived from the fiber bridging stress *vs.* COD curves of the various $SHLC^4$ incorporating PE and PP fibers, in accordance with Eqs. (3)–(6).

From the strength criterion standpoint (refer to first two rows of Table 8), the fiber bridging strength (σ_b) observations exhibited a good correlation with the results of the maximum debonding forces in the single fiber pull-out test (see Table 7). The σ_b of PP-based $SHLC^4$ decreased as the clinker content in the matrix decreased. In contrast, this trend was not evident in the reference PE-based $SHLC^4$; for instance, $SHLC^4$-35-PE exhibited a higher σ_b than $SHLC^4$-50-PE, which is in line with the observation that PE fibers exhibited better bond in the LC^3-35 matrix than in LC^3-50. Furthermore, the matrix cracking stress (σ_m) mimicked the trend of σ_b for each fiber/matrix pairing. Remarkably, the trend of σ_m in notched specimens displayed a similar pattern to that of the first crack stress in unnotched specimens subjected to tensile loads (as shown later in Section 4.5), underscoring the consistent quality of the notches among different $SHLC^4$ [63]. Consequently, $PSH_{strength}$ can be reliably estimated from the σ-δ curves – Fig. 12(a).

Examining the parameters influencing the energy criterion (see the bottom three rows of Table 8), the transition from $SHLC^4$-50 to $SHLC^4$-25 resulted in an increase in the crack opening displacement at peak fiber bridging stress (δ_b) for the PP fiber-reinforced composites. In contrast, a decrease in δ_b was observed for the PE-reinforced reference composites. δ_b consists of two deformation components: one resulting from fiber pull-out and the other from the intrinsic elongation capacity of the fibers within the crack flanks. The opposite trends in δ_b between PP and PE fibers can be attributed to differences in their mechanical properties. Indeed, PE fibers exhibit significantly higher stiffness, and a lower elongation capacity compared to the more compliant PP fibers. As

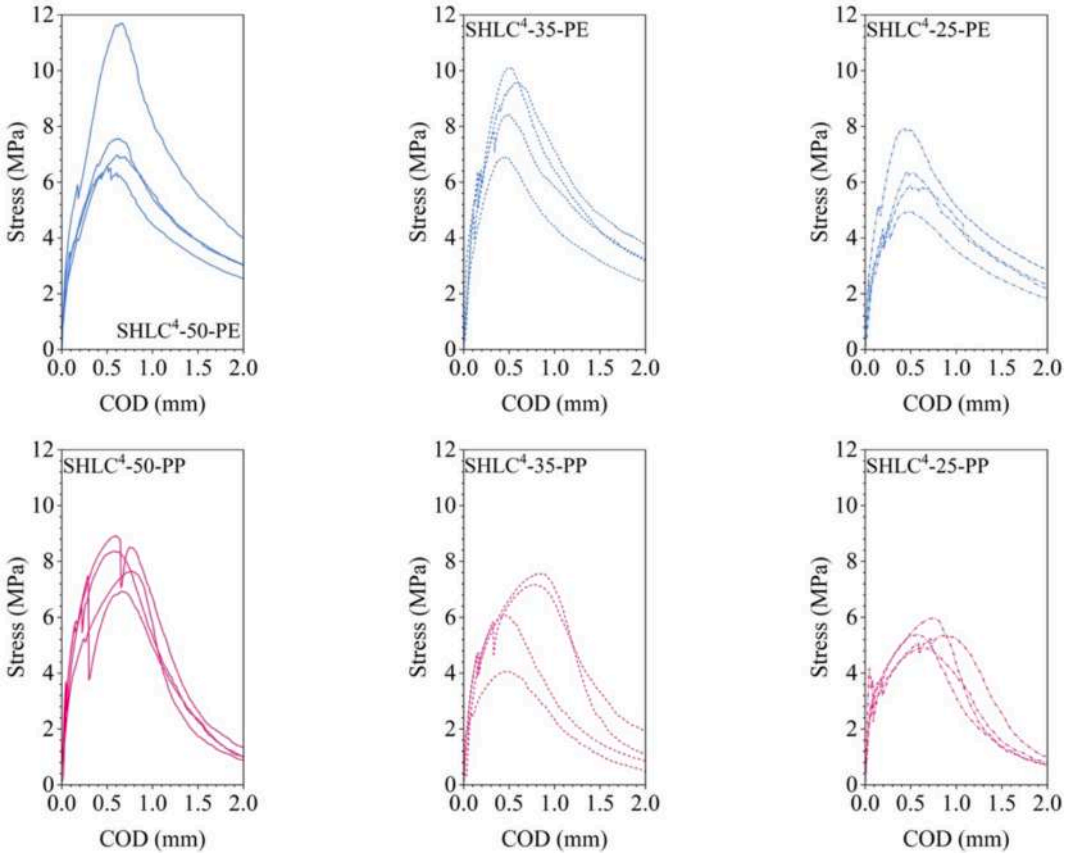

Fig. 11. Tensile fiber bridging stress *vs.* COD (σ-δ) curves of various SHLC^4 under investigation.

Table 8
Key mechanical parameters that have been ascertained through the analysis of σ-δ results derived from the uniaxial tensile test on miniature notched specimens. The standard deviation is indicated within parentheses.

Criterion	Mechanical parameters	SHLC^4-50		SHLC^4-35		SHLC^4-25	
		PE	PP	PE	PP	PE	PP
Strength	Matrix cracking stress – σ_m [MPa]	4.25 (1.12)	5.61 (0.33)	5.40 (0.91)	3.67 (1.20)	4.40 (0.48)	3.41 (0.56)
	Fiber bridging strength – σ_b [MPa]	8.20 (2.37)	8.31 (0.63)	8.75 (1.41)	6.22 (1.57)	6.29 (1.24)	5.40 (0.43)
Energy	Crack opening displacement at peak – δ_b [mm]	0.60 (0.06)	0.65 (0.10)	0.51 (0.05)	0.63 (0.20)	0.48 (0.03)	0.71 (0.12)
	Crack tip toughness – J_{tip} [N/mm]	0.22 (0.10)	0.36 (0.06)	0.31 (0.10)	0.18 (0.11)	0.30 (0.05)	0.10 (0.04)
	Complementary energy – J'_b [N/mm]	1.55 (0.70)	1.35 (0.18)	1.32 (0.33)	1.01 (0.51)	0.89 (0.21)	0.82 (0.20)

a result, PP fibers not only undergo pull-out from all matrix types but also experience considerable plastic deformation even at low applied stress. When transitioning from SHLC^4-50 to SHLC^4-25, the plastic deformation of PP fibers does not change as drastically, however, the contribution of the fiber pull-out displacement component to δ_b increases as the bond strength decreases due to the ease with which PP pulls out. Conversely, in the case of PE fibers, although their elongation capacity is limited, some fiber elongation still contributes to δ_b at higher stress levels. However, as the bond weakens, PE fibers are more easily pulled out with minimal contribution from the elongation component.

Consequently, the two J-integrals – J_{tip} and J'_b – based on Eqs. (4) and (5), respectively, were estimated. In general, J_{tip} followed the same trend as σ_m, resulting in an apparent reduction for SHLC^4-PP with reduced clinker content. Indeed, as SCMs replace more and more PC, the fracture toughness of the matrix reduces, which also leads to reduced crack tip toughness, *i.e.*, cracks can propagate easily. On the contrary, this relationship between σ_m and the matrix's clinker content did not emerge for SHLC^4-PE. Concerning J'_b, a reduction was observed for all composite types as the PC replacement was increased. Moreover, PP-based SHLC^4 consistently displayed lower values than its PE counterpart. This can be attributed to the favorable interface characteristics of the latter. However, in SHLC^4-25, the complementary energy offered by PP and PE fibers resulted in similar values, as the bond was primarily impaired by the pronounced dilution of the matrix, which equally affected the bond with both fiber types.

$PSH_{strength}$ and PSH_{energy} indices are presented in Fig. 12(a) and (b), respectively. All SHLC^4 types exhibited strength indices meeting the strength criterion ($PSH_{strength} > 1$). Kanda [78] proposed a minimum threshold of 1.2 for PE fibers in SHCC to guarantee optimal and robust strain-hardening behavior, indicated by a dashed line on the graph. This threshold was also adopted as the benchmark for PP-SHLC^4, despite the inherent shortcomings in PP performance, such as low strength and high compliance, which were partially addressed by adding 0.5 vol% of additional PP fibers. Consequently, the SHLC^4-35-PP and SHLC^4-25-PP exhibited a comparable $PSH_{strength}$ index to their PE counterparts with the corresponding matrices. The SHLC^4-50-PP exhibited the lowest

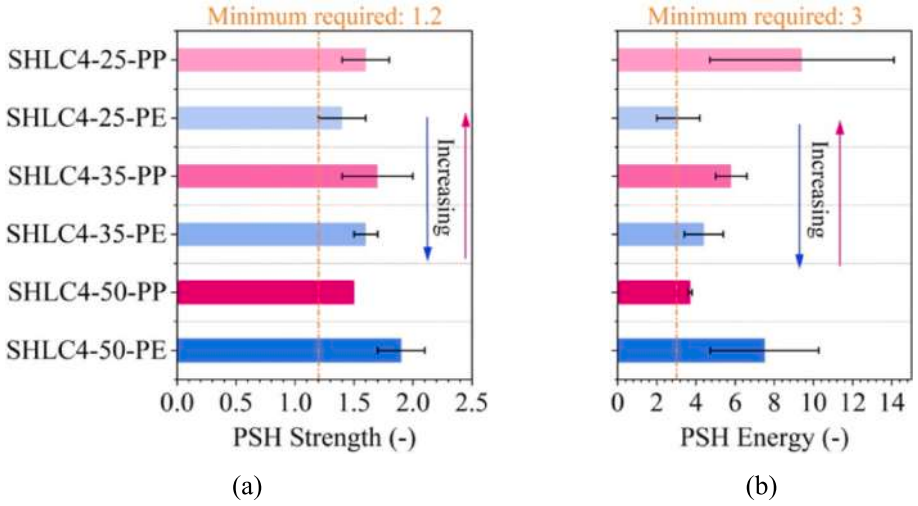

Fig. 12. PSH strength (a) and energy (b) indices of various SHLC[4] under investigation. The minimum required values are marked in orange based on Kanda's recommendations for PE fibers [78].

$PSH_{strength}$, which was attributed to the significant strength and stiffness mismatch between matrix and fibers that do not exist to a similar extent in SHLC[4]-50-PE, leading to highest $PSH_{strength}$. Nevertheless, all composites exhibited a $PSH_{strength}$ index value greater than 1.2, indicating the potential for multiple cracking for all the composites.

A similar trend, albeit more pronounced, was observed for the PSH_{energy} indices, which increased for SHLC[4]-PP as the clinker content in the matrices decreased. Furthermore, the mismatch in the PSH_{energy} indices for SHLC[4]-PP and their corresponding matrix-equivalent SHLC[4]-PE was also quite pronounced. The high compliance gap between the two fibers resulted in divergent trends for PSH_{energy} indices. In a more robust matrix, such as SHLC[4]-50, the pull-out of PP fibers is constrained. In contrast, significant plastic deformation occurs in a weaker matrix, such as SHLC[4]-25, as pull-out and plastic deformation of bridging PP fibers contribute to complementary energy. On the other hand, bridging PE fibers exhibited higher complementary energy with SHLC[4]-50 due to their high stiffness and adequate bond properties, which gradually diminished as the matrix diluted, as illustrated in Fig. 12(b). Nevertheless, all composites yielded PSH_{energy} indices above 3, which is the recommended PSH_{energy} value for bridging PE fibers according to Kanda [78].

In consideration of the aforementioned findings, it can be deduced that matrices classified as "*weak*" exhibit a better compatibility with "*compliant*" fibers, thereby meeting the established *strength* and *energy criteria* for SHCC. Conversely, matrices classified as "*strong*" demonstrate better synergy with "*stiff*" fibers. This discrepancy is primarily, but not exclusively, due to the conflicting intrinsic mechanical properties of PP and PE, which place these fibers at opposing ends of the spectrum. This assertion is further substantiated by Fig. 13, which illustrates the observed SHCC constitutive law results presented in this section. With this understanding, it is feasible to develop a customized SHCC design that optimizes performance, sustainability, and cost-effectiveness.

4.5. Uniaxial tensile tests

Fig. 14 shows the stress *vs.* strain curves from the uniaxial tensile test of the investigated SHLC[4]. Regardless of the matrix composition and reinforcing fibers, all SHLC[4] exhibited strain-hardening behavior, as

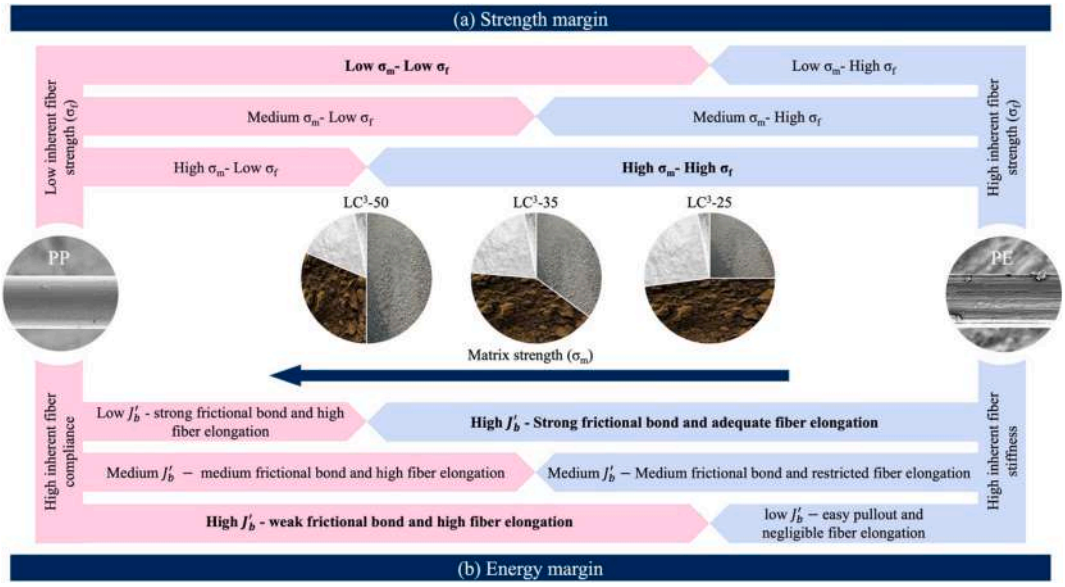

Fig. 13. Schematic illustration of strength and energy margins for different fiber/matrix pairing. The intrinsic compliance of PP and high tensile stiffness of PE fibers approach various strength classes of the matrices from opposite sides to fulfill the micromechanics-based criteria for SHCC design.

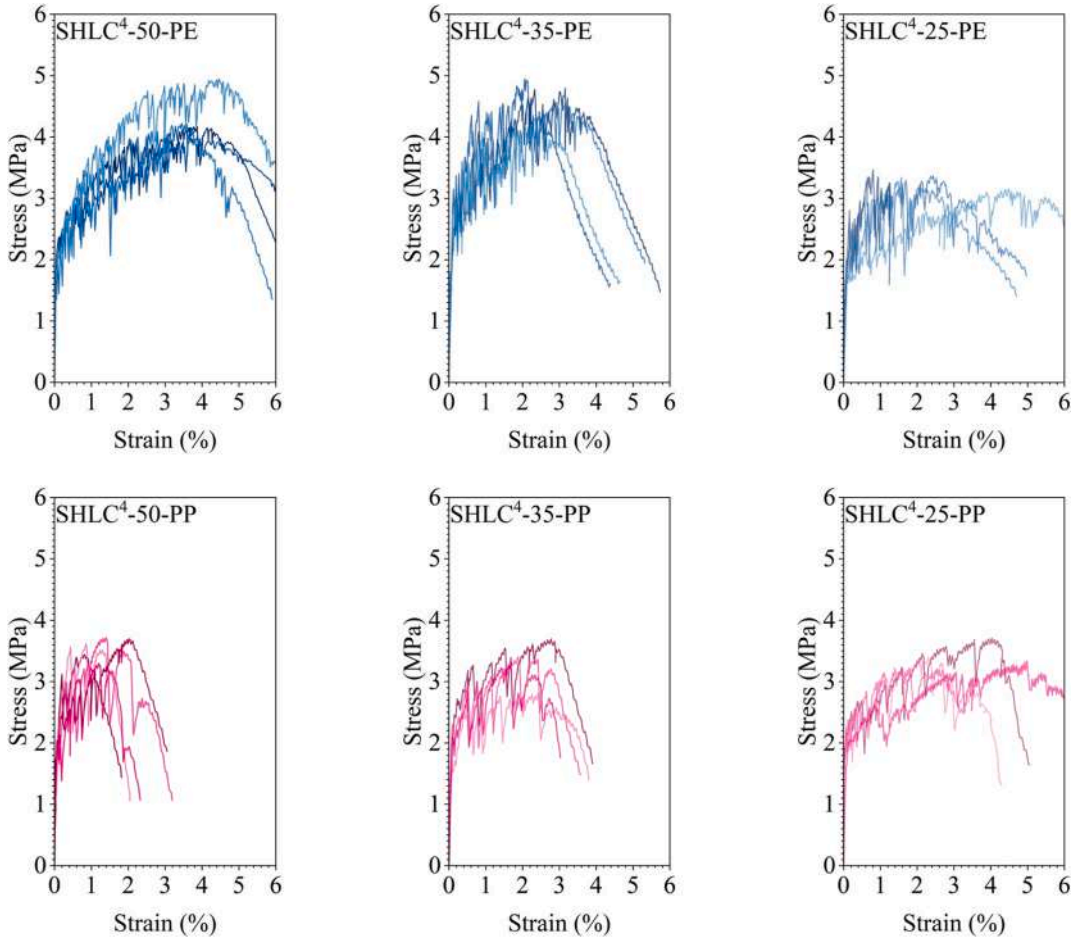

Fig. 14. Uniaxial tensile stress–strain curves of various SHLC^4 under investigation.

each combination met the *strength* and *energy criteria*. Reducing the clinker content worsened the pseudo-strain-hardening of the PE-reinforced SHLC^4 while improving it for the PP-reinforced SHLC^4. This is because these diluted matrices were designed to accommodate the compliant nature of the PP fibers rather than the relatively high stiffness of the PE fibers.

Considering the strength-related properties, *i.e.,* first crack stress (σ_{fc}) and ultimate tensile strength (σ_t), all the composites started cracking at 2 MPa or above, being in line with customary SHCC for general purposes. Generally, PP-reinforced SHLC^4 exhibited comparable σ_{fc} to PE-reinforced SHLC^4 counterparts, taking into account the standard deviations associated with each fiber/matrix pairing, see Table 9. Since σ_{fc} is primarily controlled by the mechanical response of the matrix, and in particular by the flaw sizes and their distribution in the matrix, it is nearly insensitive to the incorporated fibers. The slight variations are due to the distributions of defects, which may also vary due to manufacturing or other unavoidable uncertainties.

In terms of σ_t, SHLC^4-50-PE, and SHLC^4-35-PE outperformed their respective PP-based counterparts due to superior fiber/matrix interfacial properties. Interestingly, SHLC^4-35-PE exhibited outweighed SHLC^4-50-PE despite having a lower clinker factor due to the better fiber/matrix bonding properties. In highly diluted matrices, such as SHLC^4-25, the PP-based composite exhibited slightly higher σ_t than its PE counterpart, even though the interfacial bonding properties were comparable. This is mainly attributed to the higher volume fraction of PP fibers.

Out of the strength values measured through uniaxial tensile tests, $PSH_{strength}$ indices were evaluated once more using the σ_t/σ_{fc} ratio. This ratio is analogous to σ_b/σ_m from the σ-δ constitutive law obtained in tensile tests with notched specimens, however, without the predefined localization zone dictated by the notches, *cf.* Table 9. These results validate those obtained with the miniature notched specimens, demonstrating that the influence of handmade notches was insignificant when evaluating the σ-δ relationship in Section 4.4. The observed trends

Table 9
Summary of mechanical properties of the SHLC^4; the standard deviations are given in parentheses.

Mechanical parameters	SHLC^4-50		SHLC^4-35		SHLC^4-25	
	PE	PP	PE	PP	PE	PP
First crack stress – σ_{fc} [MPa]	2.1 (0.2)	2.7 (0.8)	2.3 (0.7)	2.0 (0.3)	1.9 (0.2)	2.0 (0.3)
Tensile strength – σ_t [MPa]	4.3 (0.4)	3.6 (0.2)	4.5 (0.3)	3.2 (0.4)	3.1 (0.4)	3.3 (0.4)
Ultimate strain – ε [%]	4.2 (0.4)	1.5 (0.5)	2.8 (0.6)	2.4 (0.4)	2.5 (1.4)	3.7 (1.0)
$PSH_{strength}$ [–]	2.0 (0.4)	1.4 (0.4)	2.1 (0.6)	1.6 (0.2)	1.6 (0.3)	1.7 (0.4)
Avg. Crack width [μm]	110.4 (20.6)	302.8 (77.2)	125.8 (14.3)	283.2 (55.2)	151.2 (39.2)	234.6 (12.3)
Crack density [/m]	297.5 (113.5)	43.0 (10.0)	236.0 (60.0)	80.0 (20.0)	187.0 (125.0)	160.0 (60.0)
Crack spacing [mm]	3.8 (1.4)	24.2 (5.7)	4.5 (1.2)	13.2 (3.7)	7.0 (3.4)	7.0 (2.7)
Work-to-fracture [kJ/m^3]	142.3 (26.9)	39.5 (17.1)	103.6 (21.0)	60.2 (18.3)	69.6 (33.8)	104.6 (34.8)

remain consistent, with a decrease and an increase in the strength of PE and PP fibers as the clinker content of the matrix was reduced from 50 % to 25 %.

The tensile strain capacity gradually increased in the PP-based SHLC^4 as the transition progressed from SHLC^4-50, SHLC^4-35, to SHLC^4-25. In contrast, the mean strain capacity of the PE-based composites gradually declined during the same transition. This finding aligns with the previously presented fiber/matrix interface results and the SHLC^4 constitutive law.

During the process of extracting the bridging PP fibers from the SHLC^4-50 matrix, the strong bond between the high-strength matrix and the low-strength and highly compliant PP fibers caused damage to the PP fibers. This increased the probability of rupture of the bridging PP fibers. Concurrently, the discrepancy between the cracking stress of the matrix and the tensile stress of the PP bridging fibers was more pronounced in SHLC^4-50-PP, thereby constraining the potential for multiple cracking and consequently reducing the overall ductility. As the matrix microstructure becomes less compact due to binder dilution, the discrepancy between the matrix strength and the bridging strength of the PP fibers broadens, as discussed in Section 4.4. Consequently, SHLC^4-25-PP exhibited the highest strain capacity of 3.7 %, accompanied by a more diffuse crack pattern (see Fig. 15(a)).

In the case of PE-based SHLC^4, SHLC^4-50-PE, and SHLC^4-35-PE exhibited the highest cracking density in line with the highest $PSH_{strength}$ index among other composite types. This also resulted in SHLC^4-50-PE exhibiting the highest strain capacity, which was 4.2 %. However, the strain capacity of SHLC^4-35-PE was reduced to 2.8 %, attributed to a relatively localized cracking pattern compared to SHLC^4-50-PE. The elevated dilution of the binder in SHLC^4-25-PE markedly impairs the interfacial bond between fibers and the matrix. This phenomenon facilitated the extraction of bridging PE fibers and restricted their elongation, ultimately leading to relatively localized damage and reduced crack density, compromising the strain capacity.

It is noteworthy that a comparable strain capacity extent is achieved by combining both the highest performance components (LC^3-50 binder and PE fibers) and the lowest performance components (LC^3-25 binder and PP fibers), the latter combination being associated with obvious environmental and economic benefits.

As illustrated in Fig. 15(b), the in-situ crack analysis was conducted using the DIC method. This analysis demonstrates the evolution and distribution of crack width (*CW*) for all SHLC^4 specimens. It is important to note that, while the maximum values in this graph represent the average *CW* at the ultimate strain, the mean and median *CWs* differ from the values reported in Table 9. This is due to the fact that the latter were derived from *CW* measurements taken at multiple strain levels (*e.g.,* 0.2 %, 0.4 %, *etc.*, up to the ultimate strain), allowing the progression of cracks to be tracked throughout the test. In particular, the median *CW* reflects the ability of the composites to regulate crack width, as opposed to the average *CW* at ultimate strain.

As can be noted, PE-based SHLC^4 demonstrated superior *CW* control in comparison to its PP-based counterparts. This outcome can be attributed to the compliance mismatch between the two fibers and the stronger interfacial bond between PE and the SHLC^4 matrix. Particularly the stronger bond between PE and SHLC^4-50 and SHLC^4-35 matrices led to establishment of higher $PSH_{strength}$ indices in these composites resulting in more saturated cracking pattern. Contrarily, the intrinsically low tensile strength of PP fibers and their relatively poor bond led to limited $PSH_{strength}$ indices, which gradually increased as the matrix becomes softer. Hence, the cracking densities in PP-based composites also increased during transition to higher replacement levels, *i.e.*, from SHLC^4-50 to SHLC^4-25. Nevertheless, all SHLC^4-PP composites exhibited higher overall *CWs* due to their significant fiber yielding. Specifically, SHLC^4-50-PP exhibits the broadest *CW* range, as the limited cracks that have formed have a greater propensity to elongate in comparison to the case where these fibers are loosely anchored to the LC^3-25 matrix, where more cracks are formed.

Overall, the poor CW control in PP-reinforced SHLC^4 remains an inherent limitation due to the compliant nature and smooth surface of PP fibers. This can raise concerns about the durability of these composites, as wider cracks may favor the ingress environmental agents (*e.g.*, chlorides), exposing the material to potential deterioration [80,81]. This problem can be mitigated by roughening the surface of the PP fibers to improve mechanical interlocking with the matrix [76,82,83] or by introducing functional groups on the PP surface to induce a better

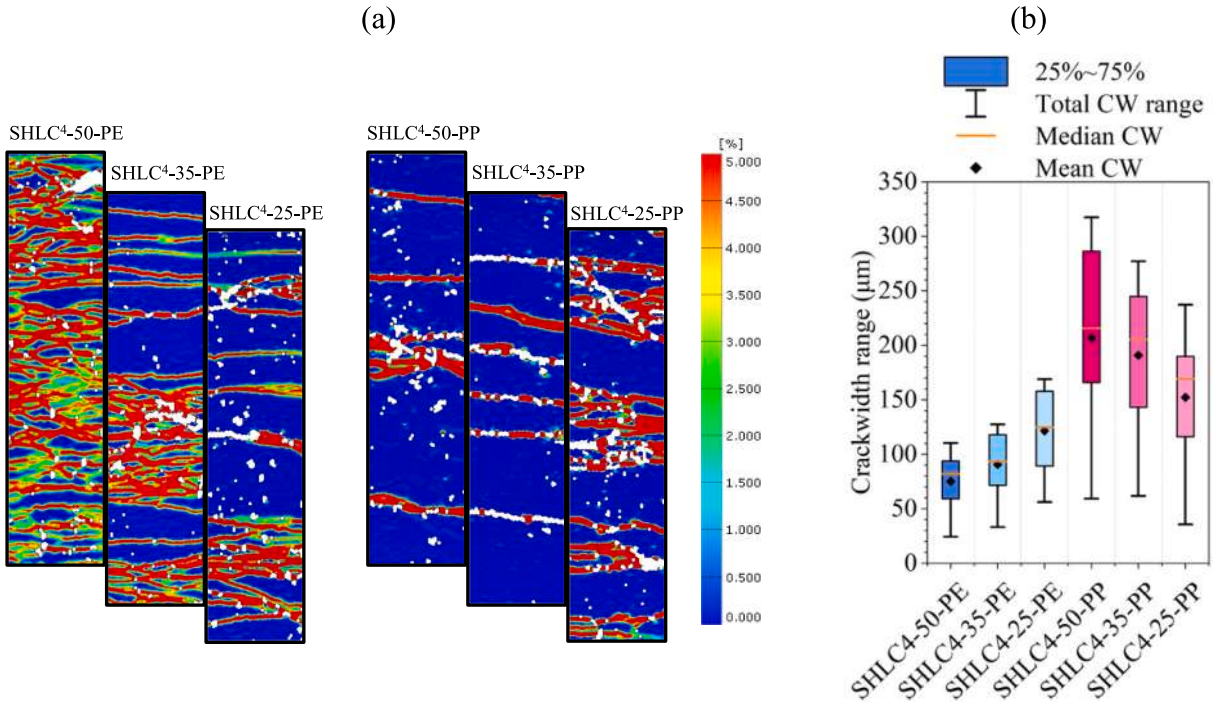

Fig. 15. (a) DIC crack pattern of different SHLC^4 at ultimate strain, the colored scale palette on the right indicates the tensile strains along the longitudinal direction, and (b) crack width distribution calculated at 0.2% strain intervals from 0.2% strain to ultimate strain of different investigated SHLC^4.

chemical bond with the cementitious matrix [74,75,84].

Fig. 16 presents the ESEM analysis conducted on the fractured surface. Different types of damage, such as fibrillation, fiber kinking, matrix micro-spalling, microcracking, abrasive scratches, *etc.*, were documented depending on the fiber and matrix type variations. When embedded in the SHLC^4-50 and SHLC^4-35 matrices, both PE and PP fiber surfaces exhibited damage due to pronounced abrasion during pull-out in the form of scratches and fibrillation, supporting the high fiber/matrix bonding characteristics. For the same reason, a relatively high extent of matrix micro-spalling was observed on the fiber surface. In addition, microcracking was observed in the orthogonal direction of the PP fiber/SHLC^4-50 matrix tunnel due to the development of high shear stresses resulting from the high compliance of PP, which tends to deform in stiff matrix that instead resists deformation. On the contrary, when PE and PP fibers were pulled out of the SHLC^4-25 matrix, a rather smooth fiber surface, similar to the original fiber surface, was observed due to the loose microstructure of the matrix and, thus, poor bond.

Notwithstanding the limitations, particularly the unfavorable high crack width control of PP-based SHLC^4, the favorable fracture toughness of SHLC^4-25-PP, in particular, makes it a promising material for application as a thin strengthening layer on existing critical infrastructure to protect against dynamic loading [15,17,19,45,85,86]. In this particular application, inadequate CW control is less significant. Indeed, the combination of a low-stiffness matrix with fibers that display high plastic deformation, such as PP or PET, is expected to perform well due to their high sensitivity to strain rate under dynamic loading conditions [16], as well as their damping potential.

5. Conclusions

This paper presents a comprehensive scale-linking experimental study targeted at the sustainable and cost-effective design of SHCC. For this purpose, PP fibers were incorporated as dispersed reinforcements in different LC^3 matrices with systematically reduced clinker contents: 50 %, 35 %, and 25 %. In parallel, high-performance PE fibers were also investigated as a benchmark. From a series of micro-, meso-, and macro-scale mechanical tests, the following conclusions were drawn:

- Although PP fibers are markedly more compliant than high-performance PE fibers, both fibers exhibited strain-hardening behavior when embedded in various LC^3-based matrices. This was achieved through a methodical approach involving the strategic modification of the matrix formulations and fiber choice, resulting in a modification of the fiber/matrix interfaces, and consequently, the fiber crack bridging capacities.
- Given PP fibers' inherently low mechanical performance, the primary challenge was to meet the requisite strength criterion to achieve the desired strain-hardening behavior. To meet this criterion, the highly diluted LC^3 matrices provided the advocated mismatch between matrix cracking stress and peak crack-bridging stress.

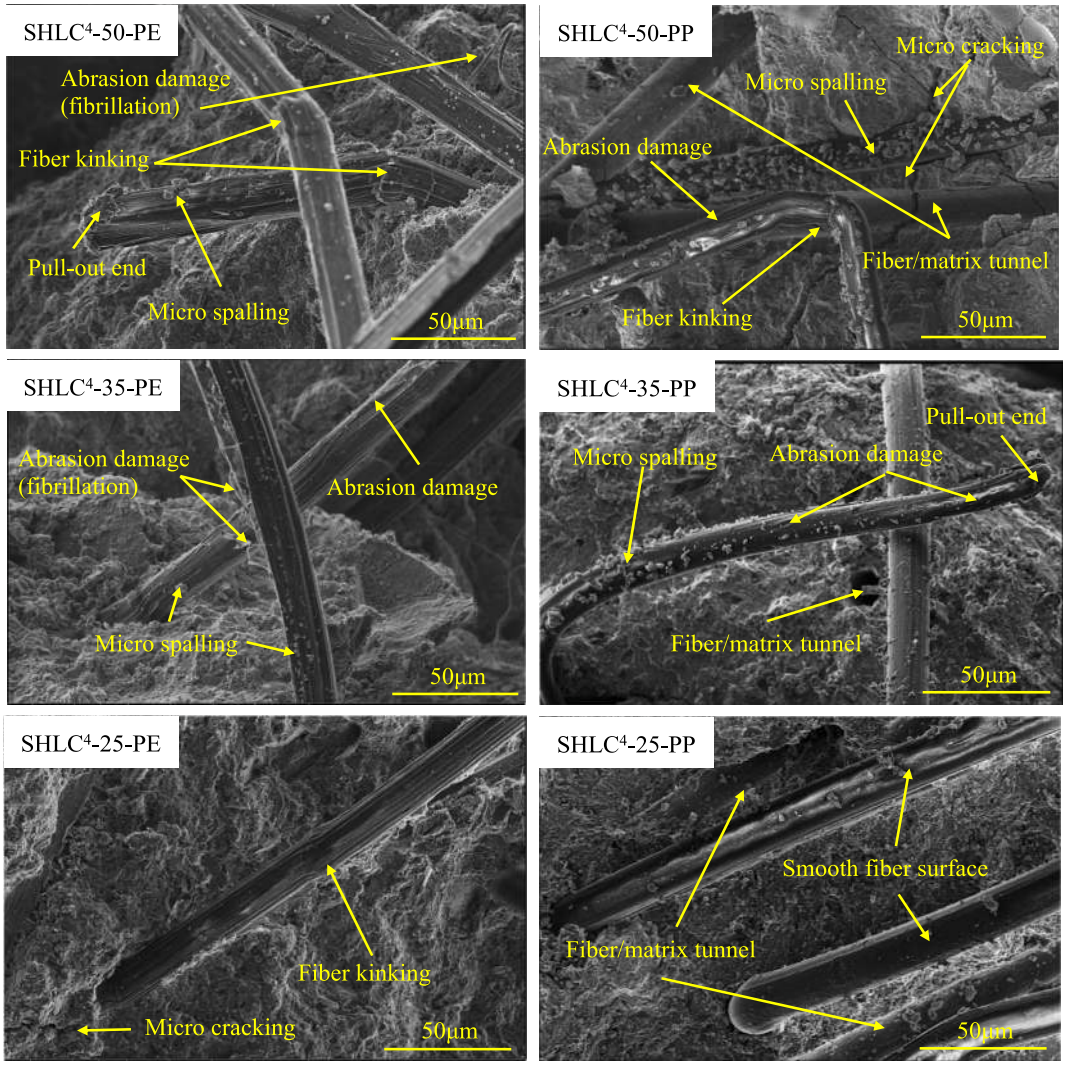

Fig. 16. SEM analysis of fractured SHLC^4 samples revealing distinct damage mechanisms influenced by matrix composition and fiber type variations.

- A substantial portion of the complementary energy of the crack-bridging PP fibers in SHLC^4 is derived from their high plastic deformation capacity, resulting from their low tenacity. The remaining contribution derives from fiber pull-out. This improves tensile ductility at the expense of crack width control in PP-based SHLC^4.
- The discrepancy between the tensile strength and stiffness of standard PP and reference PE fibers results in a notable difference in the performance of high-strength and low-strength matrices. High-strength matrices demonstrate enhanced performance when combined with high-performance fibers (PE), while low-strength matrices exhibit superior performance when used with low-performance fibers (PP).

In essence, the incorporation of low-tenacity PP fibers into an ultra-low clinker SHLC^4-25 matrix resulted in a composite with tensile strength and strain capacity that was only marginally lower than those of the high-performance PE fibers in an SHLC^4-50 matrix. The former combination offers clear environmental and economic advantages, particularly regarding the sustainability and cost-effectiveness of the SHCC.

6. Future works

While the present study provided a detailed examination of the design and development of a low-clinker, cost-effective SHCC, future research will focus on the following aspects:

- A comprehensive cradle-to-gate life cycle assessment (*LCA*) of the developed composites will be conducted, with a particular emphasis on their environmental impact and economic feasibility. This analysis will provide a holistic understanding of the sustainability benefits associated with low-clinker SHCC formulations.
- The high strain-rate behavior of the developed composites will be evaluated through uniaxial tensile testing. Testing will focus on the material response and energy dissipation capacity of the composites under impact loading conditions, to assess their feasibility as an impact-resistant material for structural applications.
- The addition of continuous carbon fabric in low-clinker SHCC is being explored to improve tensile performance and crack width control through hybrid fiber reinforcement.

CRediT authorship contribution statement

Ameer Hamza Ahmed: Writing – review & editing, Writing – original draft, Visualization, Validation, Methodology, Investigation, Formal analysis, Data curation, Conceptualization. **Julia Hübner:** Writing – review & editing, Writing – original draft, Validation, Investigation, Formal analysis, Data curation. **Dominik Junger:** Writing – review & editing, Validation, Investigation, Formal analysis, Data curation. **Cesare Signorini:** Writing – review & editing, Visualization, Validation, Methodology, Supervision. **Marko Butler:** Writing – review & editing, Validation, Supervision. **Marco Liebscher:** Writing – review & editing, Validation, Supervision, Resources, Project administration, Methodology, Conceptualization. **Christina Scheffler:** Writing – review & editing, Validation, Supervision, Resources. **Viktor Mechtcherine:** Writing – review & editing, Supervision, Resources, Project administration, Funding acquisition.

Funding

This work was financially support by the German Research Foundation (Deutsche Forschungsgemeinschaft, DFG) for their funding of project 455631638, and the Research Training Group GRK 2250/3 “Mineral-bonded composites for enhanced structural impact safety”, project 287321140.

Declaration of competing interest

The authors declare that they have no known competing financial interests or personal relationships that could have appeared to influence the work reported in this paper.

Data availability

Data will be made available on request.

References

[1] V. Li, From micromechanics to structural engineering - the design of cementitious composites for civil engineering applications, J. Struct. Mech. Earthq. Eng. 10 (1992) 37–48.
[2] E.-H. Yang, Y. Yang, V.C. Li, Use of high volumes of fly ash to improve ecc mechanical properties and material greenness, ACI Mater. J. 104 (2007). doi: 10.14359/18966.
[3] M. Maalej, T. Hashida, V.C. Li, Effect of fiber volume fraction on the off-crack-plane fracture energy in strain -hardening engineered cementitious composites, J. Am. Ceram. Soc. 78 (1995) 3369–3375, https://doi.org/10.1111/j.1151-2916.1995.tb07979.x.
[4] V.C. Li, C.K. Leung, Y.,, Steady-state and multiple cracking of short random fiber composites, J. Eng. Mech. 118 (1992) 2246–2264, https://doi.org/10.1061/(ASCE)0733-9399(1992)118:11(2246).
[5] J. Li, J. Qiu, J. Weng, E.-H. Yang, Micromechanics of engineered cementitious composites (ECC): a critical review and new insights, Constr. Build. Mater. 362 (2023) 129765, https://doi.org/10.1016/j.conbuildmat.2022.129765.
[6] M. Xu, S. Song, L. Feng, J. Zhou, H. Li, V.C. Li, Development of basalt fiber engineered cementitious composites and its mechanical properties, Constr. Build. Mater. 266 (2021) 121173, https://doi.org/10.1016/j.conbuildmat.2020.121173.
[7] N. Zhang, M. Xu, S. Song, H. Li, J. Zhou, G. Ma, Impact resistance of basalt fiber strain-hardening cementitious composites exposed to elevated temperatures, Constr. Build. Mater. 262 (2020) 120081, https://doi.org/10.1016/j.conbuildmat.2020.120081.
[8] S. Kumar, D.C. Rai, Development of engineered cementitious composite with moderate tensile properties using polyester fibers, Constr. Build. Mater. 404 (2023) 133158, https://doi.org/10.1016/j.conbuildmat.2023.133158.
[9] Y.M. Lim, V.C. Li, Durable repair of aged infrastructures using trapping mechanism of engineered cementitious composites, Cem. Concr. Compos. 19 (1997) 373–385, https://doi.org/10.1016/S0958-9465(97)00026-7.
[10] T. Kamada, V.C. Li, The effects of surface preparation on the fracture behavior of ECC/concrete repair system, (2000).
[11] S. Müller, V. Mechtcherine, Use of strain-hardening cement-based composites (SHCC) for retrofitting, MATEC Web Conf. 199 (2018) 09006, https://doi.org/10.1051/matecconf/201819909006.
[12] S. Kumar, D.C. Rai, Enhancing flexural strength of unreinforced masonry members using cementitious matrix-based composites, in: S.B. Singh, S.V. Barai (Eds.), Stab. Fail. High Perform. Compos. Struct., Springer Nature, Singapore, 2022, pp. 125–142. doi: 10.1007/978-981-19-2424-8_6.
[13] K.E. Kesner, S.L. Billington, Investigation of ductile cementbased composites for seismic strengthening and retrofit, in: Netherlands, 2001: pp. 65–72.
[14] G. Parra-Montesinos, J.K. Wight, Seismic response of exterior RC column-to-steel beam connections, J. Struct. Eng. 126 (2000) 1113–1121, https://doi.org/10.1061/(ASCE)0733-9445(2000)126:10(1113).
[15] V. Mechtcherine, O. Millon, M. Butler, K. Thoma, Mechanical behaviour of strain hardening cement-based composites under impact loading, Cem. Concr. Compos. 33 (2011) 1–11, https://doi.org/10.1016/j.cemconcomp.2010.09.018.
[16] I. Curosu, V. Mechtcherine, O. Millon, Effect of fiber properties and matrix composition on the tensile behavior of strain-hardening cement-based composites (SHCCs) subject to impact loading, Cem. Concr. Res. 82 (2016) 23–35, https://doi.org/10.1016/j.cemconres.2015.12.008.
[17] I. Curosu, V. Mechtcherine, D. Forni, E. Cadoni, Performance of various strain-hardening cement-based composites (SHCC) subject to uniaxial impact tensile loading, Cem. Concr. Res. 102 (2017) 16–28, https://doi.org/10.1016/j.cemconres.2017.08.008.
[18] A. Tawfik, C. Signorini, V. Mechtcherine, Direct assessment of the shear behavior of strain-hardening cement-based composites under quasi-static and impact loading: influence of shear span and notch depth, Cem. Concr. Compos. 140 (2023) 105119, https://doi.org/10.1016/j.cemconcomp.2023.105119.
[19] C. Signorini, F. Bracklow, M. Hering, M. Butler, L. Leicht, T. Schubert, M.A. B. Beigh, B. Beckmann, M. Curbach, V. Mechtcherine, Ballistic limit and damage assessment of hybrid fibre-reinforced cementitious thin composite plates under impact loading, J. Build. Eng. 80 (2023) 108037, https://doi.org/10.1016/j.jobe.2023.108037.
[20] V.C. Li, On Engineered Cementitious Composites (ECC)- A Review of the Material and Its Applications, 1 (2003).
[21] K. Scrivener, F. Martirena, S. Bishnoi, S. Maity, Calcined clay limestone cements (LC3), Cem. Concr. Res. 114 (2018) 49–56, https://doi.org/10.1016/j.cemconres.2017.08.017.

[22] M. Antoni, J. Rossen, F. Martirena, K. Scrivener, Cement substitution by a combination of metakaolin and limestone, Cem. Concr. Res. 42 (2012) 1579–1589, https://doi.org/10.1016/j.cemconres.2012.09.006.

[23] M. Sharma, S. Bishnoi, F. Martirena, K. Scrivener, Limestone calcined clay cement and concrete:a state-of-the-art review, Cem. Concr. Res. 149 (2021) 106564, https://doi.org/10.1016/j.cemconres.2021.106564.

[24] D. Zhang, B. Jaworska, H. Zhu, K. Dahlquist, V.C. Li, Engineered Cementitious Composites (ECC) with limestone calcined clay cement (LC3), Cem. Concr. Compos. 114 (2020) 103766, https://doi.org/10.1016/j.cemconcomp.2020.103766.

[25] L. Wang, N. Ur Rehman, I. Curosu, Z. Zhu, M.A.B. Beigh, M. Liebscher, L. Chen, D. C.W. Tsang, S. Hempel, V. Mechtcherine, On the use of limestone calcined clay cement (LC3) in high-strength strain-hardening cement-based composites (HS-SHCC), Cem. Concr. Res. 144 (2021) 106421, https://doi.org/10.1016/j.cemconres.2021.106421.

[26] J. Yu, H.-L. Wu, C.K.Y. Leung, Feasibility of using ultrahigh-volume limestone-calcined clay blend to develop sustainable medium-strength Engineered Cementitious Composites (ECC), J. Clean. Prod. 262 (2020) 121343, https://doi.org/10.1016/j.jclepro.2020.121343.

[27] G. Gong, M. Guo, Y. Zhou, S. Zheng, B. Hu, Z. Zhu, Z. Huang, Multiscale investigation on the performance of engineered cementitious composites incorporating PE fiber and limstone calcined clay cement (LC3), Polymers 14 (2022) 1291, https://doi.org/10.3390/polym14071291.

[28] Y. Zhou, G. Gong, B. Xi, M. Guo, F. Xing, C. Chen, Sustainable lightweight engineered cementitious composites using limestone calcined clay cement (LC3), Compos. B Eng. 243 (2022) 110183, https://doi.org/10.1016/j.compositesb.2022.110183.

[29] A.H. Ahmed, M. Liebscher, V. Mechtcherine, Mechanical performance of strain hardening limestone calcined clay cementitious composites (SHLC4) subject to wet-dry cycles, in: M. Kunieda, T. Kanakubo, T. Kanda, K. Kobayashi (Eds.), Strain Hardening Cem. Compos., Springer International Publishing, Cham, 2023: pp. 3–12. doi: 10.1007/978-3-031-15805-6_1.

[30] L. Wang, Z. Zhu, A. Hamza Ahmed, M. Liebscher, X. Zhu, V. Mechtcherine, Self-healing behavior of high-strength strain-hardening cement-based composites (HS-SHCC) blended with limestone calcined clay cement (LC3), Constr. Build. Mater. 370 (2023) 130633, https://doi.org/10.1016/j.conbuildmat.2023.130633.

[31] H. Zhu, D. Zhang, T. Wang, M. McBain, V.C. Li, Intrinsic self-stressing and low carbon Engineered Cementitious Composites (ECC) for improved sustainability, Cem. Concr. Res. 149 (2021) 106580, https://doi.org/10.1016/j.cemconres.2021.106580.

[32] Q. Liao, J.-T. Yu, F.-Y. Dong, R. Fediuk, K.-Q. Yu, Tension-shear characteristics, cost and environmental impact of polyethylene fiber reinforced engineered cementitious composites: the role of fiber content, Constr. Build. Mater. 428 (2024) 136312, https://doi.org/10.1016/j.conbuildmat.2024.136312.

[33] V. Li, C. Wu, S. Wang, A. Ogawa, T. Saito, Interface tailoring for strain-hardening polyvinyl alcohol-engineered cementitious composite (PVA-ECC), ACI Mater. J. 99 (2002) 463–472.

[34] Textile Exchange, Preferred fiber & Materials Market Report, 2022. https://textileexchange.org/app/uploads/2022/10/Textile-Exchange_PFMR_2022.pdf (accessed May 17, 2023).

[35] D. Zhang, J. Yu, H. Wu, B. Jaworska, B.R. Ellis, V.C. Li, Discontinuous micro-fibers as intrinsic reinforcement for ductile Engineered Cementitious Composites (ECC), Compos. B Eng. 184 (2020) 107741, https://doi.org/10.1016/j.compositesb.2020.107741.

[36] C. Signorini, S. Marinelli, V. Volpini, A. Nobili, E. Radi, B. Rimini, Performance of concrete reinforced with synthetic fibres obtained from recycling end-of-life sport pitches, J. Build. Eng. 53 (2022) 104522, https://doi.org/10.1016/j.jobe.2022.104522.

[37] R. Hufenus, Y. Yan, M. Dauner, T. Kikutani, Melt-spun fibers for textile applications, Materials 13 (2020) 4298, https://doi.org/10.3390/ma13194298.

[38] A.H. Ahmed, C. Signorini, M. Chikhradze, M. Liebscher, M. Butler, V. Mechtcherine, Employing limestone and calcined clay for preserving the strain-hardening response of PET fiber-reinforced cementitious composites, Constr. Build. Mater. 438 (2024) 137166, https://doi.org/10.1016/j.conbuildmat.2024.137166.

[39] E.-H. Yang, V.C. Li, Strain-hardening fiber cement optimization and component tailoring by means of a micromechanical model, Constr. Build. Mater. 24 (2010) 130–139, https://doi.org/10.1016/j.conbuildmat.2007.05.014.

[40] B. Felekoglu, K. Tosun-Felekoglu, R. Ranade, Q. Zhang, V.C. Li, Influence of matrix flowability, fiber mixing procedure, and curing conditions on the mechanical performance of HTPP-ECC, Compos. B Eng. 60 (2014) 359–370, https://doi.org/10.1016/j.compositesb.2013.12.076.

[41] D. Zhang, H. Zhu, M. Hou, K.E. Kurtis, P.J.M. Monteiro, V.C. Li, Optimization of matrix viscosity improves polypropylene fiber dispersion and properties of engineered cementitious composites, Constr. Build. Mater. 346 (2022) 128459, https://doi.org/10.1016/j.conbuildmat.2022.128459.

[42] H. Zhu, D. Zhang, T. Wang, H. Wu, V.C. Li, Mechanical and self-healing behavior of low carbon engineered cementitious composites reinforced with PP-fibers, Constr. Build. Mater. 259 (2020) 119805, https://doi.org/10.1016/j.conbuildmat.2020.119805.

[43] J.P. Modrak, High tenacity, high elongation polypropylene fibers, their manufacture, and use, US5846654A, 1998. https://patents.google.com/patent/US5846654A/en (accessed March 25, 2024).

[44] S. Ikai, J.R. Reichert, A.V. Rodrigues, V.A. Zampieri, Asbestos-free technology with new high toughness polypropylene (PP) fibers in air-cured Hatschek process, Constr. Build. Mater. 24 (2010) 171–180, https://doi.org/10.1016/j.conbuildmat.2009.06.019.

[45] I. Curosu, V. Mechtcherine, M. Hering, M. Curbach, Mineral-bonded composites for enhanced structural impact safety - Overview of the format, goals and achievements of the research group GRK 2250, in: Proc. 10th Int. Conf. Fract. Mech. Concr. Concr. Struct., IA-FraMCoS, 2019. doi: 10.21012/FC10.235408.

[46] A. Peled, E. Zaguri, G. Marom, Bonding characteristics of multifilament polymer yarns and cement matrices, Compos. Part Appl. Sci. Manuf. 39 (2008) 930–939, https://doi.org/10.1016/j.compositesa.2008.03.012.

[47] C. Signorini, A. Sola, B. Malchiodi, A. Nobili, Highly dissipative fiber-reinforced concrete for structural screeds, J. Mater. Civ. Eng. 34 (2022) 04022022, https://doi.org/10.1061/(ASCE)MT.1943-5533.0004160.

[48] E.-H. Yang, S. Wang, Y. Yang, V.C. Li, Fiber-bridging constitutive law of engineered cementitious composites, J. Adv. Concr. Technol. 6 (2008) 181–193, https://doi.org/10.3151/jact.6.181.

[49] C.K.Y. Leung, Y. Geng, Effect of lateral stresses on fiber debonding/pull-out, Compos. Eng. 5 (1995) 1331–1348, https://doi.org/10.1016/0961-9526(95)00064-T.

[50] J. Ma, D. Wang, S. Zhao, P. Duan, S. Yang, Influence of particle morphology of ground fly ash on the fluidity and strength of cement paste, Materials 14 (2021) 283, https://doi.org/10.3390/ma14020283.

[51] A.H. Ahmed, M. Liebscher, C. Signorini, V. Mechtcherine, investigating the potential of limestone and calcined clay as a substitute for fly ash in strain-hardening cementitious composites (SHCC), ACI Symp. Publ. 362 (2024). doi: 10.14359/51740893.

[52] BS EN 197-1, Cement - Composition, specifications and conformity criteria for common cements, British Standards Institution, London, 2011. https://knowledge.bsigroup.com/products/cement-composition-specifications-and-conformity-criteria-for-common-cements/standard (accessed April 16, 2023).

[53] P.A.B. Carstens, S.A. Marais, C.J. Thompson, Improved and novel surface fluorinated products, J. Fluor. Chem. 104 (2000) 97–107, https://doi.org/10.1016/S0022-1139(00)00232-3.

[54] Z. Zheng, D. Feldman, Synthetic fibre-reinforced concrete, Prog. Polym. Sci. 20 (1995) 185–210, https://doi.org/10.1016/0079-6700(94)00030-6.

[55] Dyneema® Fact Sheets by EuroFibers - Issuu, (2012). https://issuu.com/eurofibers/docs/name8f0d44 (accessed May 17, 2023).

[56] Polypropylene (PP) Fibres, IFG - Int. Fibres Group (n.d.). https://fibresgroup.com/products/pp/ (accessed May 17, 2023).

[57] Y. Li, J. Li, E.-H. Yang, X. Guan, Mechanism study of crack propagation in river sand Engineered Cementitious Composites (ECC), Cem. Concr. Compos. 128 (2022) 104434, https://doi.org/10.1016/j.cemconcomp.2022.104434.

[58] A.H. Ahmed, S. Nune, M. Liebscher, T. Köberle, A. Willomitzer, I. Noack, M. Butler, V. Mechtcherine, Exploring the role of dilutive effects on microstructural development and hydration kinetics of limestone calcined clay cement (LC3) made of low-grade raw materials, J. Clean. Prod. (2023) 139438, https://doi.org/10.1016/j.jclepro.2023.139438.

[59] M. Ranjbarian, V. Mechtcherine, A novel test setup for the characterization of bridging behaviour of single microfibres embedded in a mineral-based matrix, Cem. Concr. Compos. 92 (2018) 92–101, https://doi.org/10.1016/j.cemconcomp.2018.05.017.

[60] DIN EN 196-1:2016-11, Prüfverfahren für Zement_- Teil_1: Bestimmung der Festigkeit; Deutsche Fassung EN_196-1:2016, 2016, doi: 10.31030/2482416.

[61] C. Scheffler, S. Zhandarov, E. Mäder, Alkali resistant glass fiber reinforced concrete: pull-out investigation of interphase behavior under quasi-static and high rate loading, Cem. Concr. Compos. 84 (2017) 19–27, https://doi.org/10.1016/j.cemconcomp.2017.08.009.

[62] E. Wölfel, H. Brünig, I. Curosu, V. Mechtcherine, C. Scheffler, Dynamic single-fiber pull-out of polypropylene fibers produced with different mechanical and surface properties for concrete reinforcement, Materials 14 (2021) 722, https://doi.org/10.3390/ma14040722.

[63] I. Curosu, E. Muja, M. Ismailov, A.H. Ahmed, M. Liebscher, V. Mechtcherine, An experimental-analytical scale-linking study on the crack-bridging mechanisms in different types of SHCC in dependence on fiber orientation, Cem. Concr. Res. 152 (2022) 106650, https://doi.org/10.1016/j.cemconres.2021.106650.

[64] R. Lorenzoni, I. Curosu, S. Paciornik, V. Mechtcherine, M. Oppermann, F. Silva, Semantic segmentation of the micro-structure of strain-hardening cement-based composites (SHCC) by applying deep learning on micro-computed tomography scans, Cem. Concr. Compos. 108 (2020) 103551, https://doi.org/10.1016/j.cemconcomp.2020.103551.

[65] R. Lorenzoni, I. Curosu, F. Léonard, S. Paciornik, V. Mechtcherine, F.A. Silva, G. Bruno, Combined mechanical and 3D-microstructural analysis of strain-hardening cement-based composites (SHCC) by *in-situ* X-ray microtomography, Cem. Concr. Res. 136 (2020) 106139, https://doi.org/10.1016/j.cemconres.2020.106139.

[66] The Science of Dyneema®, (n.d.). https://www.dyneema.com/experience-more/the-science-of-dyneema (accessed May 29, 2024).

[67] J. Juijn, A.D. Vries, Fibers melt-spun from a thermoplastic alternating copolymer and a process for preparing such fibers, US20010030010A1, 2001. https://patents.google.com/patent/US20010030010A1/en (accessed May 29, 2024).

[68] H. Xu, M. An, Y. Lv, L. Zhang, Z. Wang, Structural development of gel-spinning UHMWPE fibers through industrial hot-drawing process analyzed by small/wide-angle X-ray scattering, Polym. Bull. 74 (2017) 721–736, https://doi.org/10.1007/s00289-016-1742-z.

[69] P.-C. Aitcin, Cements of yesterday and today: concrete of tomorrow, Cem. Concr. Res. 30 (2000) 1349–1359, https://doi.org/10.1016/S0008-8846(00)00365-3.

[70] I. Curosu, M. Liebscher, V. Mechtcherine, C. Bellmann, S. Michel, Tensile behavior of high-strength strain-hardening cement-based composites (HS-SHCC) made with

high-performance polyethylene, aramid and PBO fibers, Cem. Concr. Res. 98 (2017) 71–81, https://doi.org/10.1016/j.cemconres.2017.04.004.
[71] T. Gong, A.H. Ahmed, I. Curosu, V. Mechtcherine, Tensile behavior of hybrid fiber reinforced composites made of strain-hardening cement-based composites (SHCC) and carbon textile, Constr. Build. Mater. 262 (2020) 120913, https://doi.org/10.1016/j.conbuildmat.2020.120913.
[72] E. Berodier, K. Scrivener, Understanding the filler effect on the nucleation and growth of C-S-H, J. Am. Ceram. Soc. 97 (2014) 3764–3773, https://doi.org/10.1111/jace.13177.
[73] F. Zunino, K. Scrivener, Insights on the role of alumina content and the filler effect on the sulfate requirement of PC and blended cements, Cem. Concr. Res. 160 (2022) 106929, https://doi.org/10.1016/j.cemconres.2022.106929.
[74] M. Mohammadi, A. Bashiri Rezaie, M. Liebscher, T. Köberle, A. Drechsler, R. Frenzel, F. Simon, A. Synytska, V. Mechtcherine, Interfacial properties of high-strength, limestone-calcined clay cement (LC3) matrix and PE fibers, surface-modified using dopamine and tannic acid, Constr. Build. Mater. 408 (2023) 133537, https://doi.org/10.1016/j.conbuildmat.2023.133537.
[75] A. Bashiri Rezaie, M. Liebscher, M. Ranjbarian, F. Simon, C. Zimmerer, A. Drechsler, R. Frenzel, A. Synytska, V. Mechtcherine, Enhancing the interfacial bonding between PE fibers and cementitious matrices through polydopamine surface modification, Compos. B Eng. 217 (2021) 108817, https://doi.org/10.1016/j.compositesb.2021.108817.
[76] M.-M. Popa, A. Leuteritz, M. Stommel, I. Kühnert, V. Mechtcherine, C. Scheffler, Micromechanical study on polypropylene-bicomponent fibers to improve mechanical interlocking for application in strain-hardening cement-based composites, Cem. Concr. Compos. 142 (2023) 105181, https://doi.org/10.1016/j.cemconcomp.2023.105181.
[77] C.K. Leung, Y.,, Design Criteria for Pseudoductile Fiber-Reinforced Composites, J. Eng. Mech. 122 (1996) 10–18, https://doi.org/10.1061/(ASCE)0733-9399(1996)122:1(10).
[78] T. Kanda, Design of engineered cementitious composites for ductile seismic resistant elements, (1998).
[79] D.B. Marshall, B.N. Cox, A J-integral method for calculating steady-state matrix cracking stresses in composites, Mech. Mater. 7 (1988) 127–133, https://doi.org/10.1016/0167-6636(88)90011-7.
[80] G.P.A.G. Van Zijl, V. Slowik, eds., A Framework for Durability Design with Strain-Hardening Cement-Based Composites (SHCC), Springer Netherlands, Dordrecht, 2017. doi: 10.1007/978-94-024-1013-6.
[81] C. Signorini, A. Nobili, Durability of fibre-reinforced cementitious composites (FRCC) including recycled synthetic fibres and rubber aggregates, Appl. Eng. Sci. 9 (2022) 100077, https://doi.org/10.1016/J.APPLES.2021.100077.
[82] H. Pakravan, M. Jamshidi, M. Latifi, The effect of hybridization and geometry of polypropylene fibers on engineered cementitious composites reinforced by polyvinyl alcohol fibers, J. Compos. Mater. 50 (2016) 1007–1020, https://doi.org/10.1177/0021998315586078.
[83] M.-M. Popa, H. Brünig, I. Curosu, V. Mechtcherine, C. Scheffler, Spinability and characteristics of particle-shell PP-bicomponent fibers for crack bridging in mineral-bonded composites, in: P. Serna, A. Llano-Torre, J.R. Martí-Vargas, J. Navarro-Gregori (Eds.), Fibre Reinf. Concr. Improv. Innov. II, Springer International Publishing, Cham, 2022, pp. 255–264. doi: 10.1007/978-3-030-83719-8_23.
[84] A. Bashiri Rezaie, M. Liebscher, A. Drechsler, A. Synytska, V. Mechtcherine, Tannic acid/ethanolamine modification of PE fiber surfaces for improved interactions with cementitious matrices, Cem. Concr. Compos. 131 (2022) 104573, https://doi.org/10.1016/j.cemconcomp.2022.104573.
[85] M. Hering, M. Curbach, Strengthening of RC plates with mineral-bonded composite layers for enhanced impact safety, MATEC Web Conf. 323 (2020) 01015, https://doi.org/10.1051/matecconf/202032301015.
[86] V. Mechtcherine, Novel cement-based composites for the strengthening and repair of concrete structures, Constr. Build. Mater. 41 (2013) 365–373, https://doi.org/10.1016/j.conbuildmat.2012.11.117.